

# Chapter 3

## The IDEMIX Model: Parameterization of Internal Gravity Waves for Circulation Models of Ocean and Atmosphere



Dirk Olbers, Carsten Eden, Erich Becker, Friederike Pollmann  
and Johann Jungclaus

**Abstract** The IDEMIX concept is an energetically consistent framework to describe wave effects in circulation models of ocean and atmosphere. It is based on the radiative transfer equation for an internal gravity wave field in physical and wavenumber space and was shown to be successful for ocean applications. An improved IDEMIX model for the ocean will be constructed and extended by a new high-frequency, high vertical wavenumber compartment, forcing by mesoscale eddy dissipation, anisotropic tidal forcing, and wave–mean flow interaction. It will be validated using observational and model estimates. A novel concept for gravity wave parameterization in atmospheric circulation models is developed. As for the ocean, the wave field is represented by the wave energy density in physical and wavenumber space, and its prognostic computation is performed by the radiative transfer equation. This new concept goes far beyond conventional gravity wave schemes which are based on the single-column approximation and, in particular, on the strong assumptions of a stationary mean flow and a stationary wave energy equation. The radiative transfer equation has—to our knowledge—never been considered in the atmospheric

---

D. Olbers (✉)

Alfred Wegener Institute for Polar and Marine Research (AWI), Bremerhaven, Germany  
e-mail: [dirk.olbers@awi.de](mailto:dirk.olbers@awi.de)

D. Olbers

MARUM/Institut für Umweltphysik, Universität Bremen, Bremen, Germany

C. Eden · F. Pollmann

Center for Earth System Research and Sustainability (CEN), Universität Hamburg,  
Hamburg, Germany  
e-mail: [carsten.eden@uni-hamburg.de](mailto:carsten.eden@uni-hamburg.de)

F. Pollmann

e-mail: [friederike.pollmann@uni-hamburg.de](mailto:friederike.pollmann@uni-hamburg.de)

E. Becker

Leibniz-Institut für Atmosphärenphysik e.V., Universität Rostock, Rostock, Germany  
e-mail: [becker@iap-kborn.de](mailto:becker@iap-kborn.de)

J. Jungclaus

Max-Planck-Institut für Meteorologie (MPI-M), Hamburg, Germany  
e-mail: [johann.jungclaus@mpimet.mpg.de](mailto:johann.jungclaus@mpimet.mpg.de)

© Springer Nature Switzerland AG 2019

C. Eden and A. Iske (eds.), *Energy Transfers in Atmosphere and Ocean*,  
Mathematics of Planet Earth 1, [https://doi.org/10.1007/978-3-030-05704-6\\_3](https://doi.org/10.1007/978-3-030-05704-6_3)

community as a framework for subgrid-scale parameterization. The proposed parameterization will, for the first time, (1) include all relevant sources continuously in space and time and (2) accommodate all gravity wave sources (orography, fronts, and convection) in a single parameterization framework. Moreover, the new scheme is formulated in a precisely energy-preserving fashion. The project will contribute to a transfer of knowledge from the oceanic community to the atmospheric community and vice versa. We give a brief description of the oceanic and atmospheric internal wave fields, the most important processes of generation and interactions, and the ingredients of the model IDEMIX.

### 3.1 Internal Waves in Ocean and Atmosphere

Internal gravity waves arise in a stably stratified fluid through the restoring force of gravity on fluid particles displaced from their equilibrium levels. Interfacial waves occurring between two superposed layers of different density are a familiar phenomenon, in particular at the upper free surface of the ocean in form of surface waves. In the continuously stratified interior of the ocean, the restoring force of gravity is much weaker (by a factor  $\delta\rho/\rho = 10^{-3}$ , where  $\delta\rho$  is a typical density perturbation of the mean density  $\rho$ ), and the periods and wavelengths of internal waves are much larger than those of surface gravity waves. In the spectrum of oceanic motions, internal gravity waves are embedded between (and partly overlap with) small-scale three-dimensional turbulence and the geostrophic balanced motion of the oceanic eddy field, as depicted in Figure 3.1. The timescales of baroclinic gravity waves are sharply defined as being in between the stability frequency  $N \sim \delta\rho/\rho$ , called Brunt-Väisälä frequency and related to the buoyancy force, and the Coriolis frequency  $f$ , related to the Earth rotation and Coriolis force. Spatial scales can range from global scales in case of long barotropic gravity waves down to a couple of 10 m for the baroclinic gravity wave branch. On even smaller time and space scales, the internal wave regime approaches isotropic turbulence which then connects to the regime of ultimate dissipation of energy by molecular processes. Atmospheric gravity waves obey the same constraints in frequency as oceanic ones; however, dominant wavelengths are generally larger: spectra of vertical wavelength peak at 2 to 5 km in the lower stratosphere and increase to 10 to 30 km in the mesopause. Contrary to the ocean where we always see a continuum in frequency–wavenumber space, there is ample evidence that atmospheric spectra are often composed of only a few waves (see, e.g., Fritts and Alexander 2003).

Waves are an essentially linear disturbance of the wave-carrying medium: once they are generated, they propagate almost freely along their rays, as depicted in Figure 3.2, slowly changing by non-linear effects and coupling to their supporting background, thereby slowly losing attributes acquired during their particular generation process. Strongly non-linear effects such as breaking occur only as very localized events in space and time. A linear wave is characterized by an amplitude  $a(\mathbf{K})$ , and

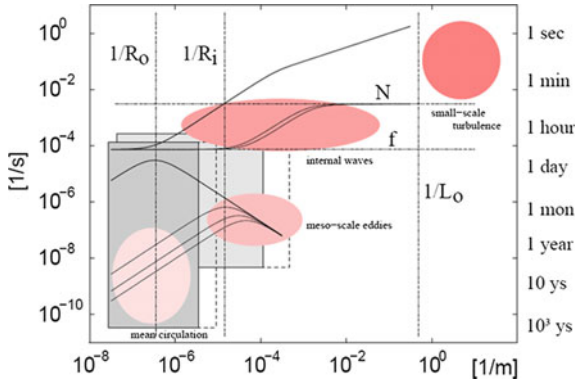
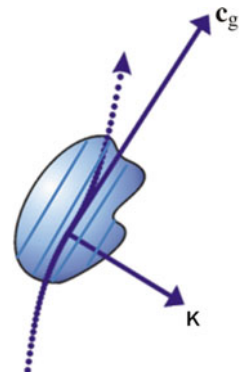


**Fig. 3.1** Space-timescales of important oceanic processes (pink areas) and scales explicitly resolved by ocean models (grey rectangular areas). The lower left rectangle represents modern global ocean climate models and the upper right rectangle eddy-resolving basin-scale models. Also shown are dispersion curves (solid lines) for linear gravity waves (upper set) and planetary waves (lower set). Vertical dotted lines indicate the external ( $R_o$ ) and the first internal ( $R_i$ ) Rossby radii and the Ozmidov length scale  $L_o$

**Fig. 3.2** Sketch of wave packet propagation along a ray. A perpendicular orientation of  $\mathbf{K}$  and the intrinsic group velocity  $\mathbf{c}_g = \partial_{\mathbf{K}}\Omega$ , as depicted here, is realized by internal gravity waves. Wave crests and troughs are orthogonal to  $\mathbf{K}$ , and these phase lines show propagation along  $\mathbf{K}$



a wave vector  $\mathbf{K}$  and an intrinsic<sup>1</sup> frequency  $\omega$ , which are related by a dispersion relation  $\omega = \Omega(\mathbf{K})$ . For internal waves

$$\omega = \Omega(\mathbf{K}) = \left( \frac{N^2 k^2 + f^2 m^2}{k^2 + m^2} \right)^{1/2} \tag{3.1}$$

where the three-dimensional wave vector  $\mathbf{K} = (\mathbf{k}, m)$  is split into the horizontal and vertical components, and  $k = |\mathbf{k}|$ . Correspondingly, we will use  $\mathbf{X} = (\mathbf{x}, z)$  for the position vector. Large-scale inhomogeneities (compared to period and wavelength) of

<sup>1</sup>We denote by  $\omega$  the intrinsic frequency, i.e. the frequency observed relative to a mean flow. Then, the Doppler shifted frequency of encounter,  $\omega_{enc} = \omega + \mathbf{K} \cdot \mathbf{U}$ , is the one observed at a fixed position in space.

the wave-carrying background can be treated by WKB methods (see, e.g., Berry and Mount 1972; Bender and Orszag 1978). Such inhomogeneities arise via a space and time-dependent Brunt-Väisälä frequency, and mean current, and a spatially varying Coriolis frequency. Waves then appear in the form of slowly varying wavetrains which may be represented locally by wave groups (or packets) characterized by a local dispersion relation  $\omega = \Omega(\mathbf{K}, \mathbf{X}, t)$  where  $\mathbf{X}$  is the spatial coordinate and  $t$  is time. A mean current  $\mathbf{U}(\mathbf{X}, t)$  is included as a Doppler shift so that  $\omega_{enc} = \omega + \mathbf{K} \cdot \mathbf{U}$  represents the frequency of encounter. A wave group propagates with the group velocity

$$\dot{\mathbf{X}} = \partial_{\mathbf{K}}\Omega + \mathbf{U} = \mathbf{V} + \mathbf{U} \quad (3.2)$$

where  $\mathbf{V} = \partial_{\mathbf{K}}\Omega$  is the intrinsic group velocity. The wave vector changes along the trajectory (ray) according to

$$\dot{\mathbf{K}} = -\partial_{\mathbf{X}}\Omega - \mathbf{K} \cdot (\nabla\mathbf{U}) \quad (3.3)$$

The process is called refraction. Here,  $\mathbf{K}$  contracts with  $\mathbf{U}$ . The influence of the mean flow in these expressions takes place via simple advection (in (3.2)) and the gradient matrix of the mean current (in (3.3)). The vertical mean current is usually negligible so that  $\mathbf{U} = (U, V, 0)$ . The intrinsic group velocity  $\mathbf{V}$  for internal waves has a peculiar property:  $\partial_{\mathbf{K}}\Omega$  is perpendicular to the wave vector  $\mathbf{K}$  (the group propagation is orthogonal to the phase propagation), and because the horizontal component  $\partial_{\mathbf{K}}\Omega$  is aligned with the horizontal wave vector  $\mathbf{k}$ , the vertical component is opposed to the vertical wavenumber,  $\partial_m\Omega \sim -\text{sign } m$ . This property is important for the IDEMIX equations (see Section 3.2). The intrinsic refraction,  $-\partial_{\mathbf{X}}\Omega$ , mainly arises from a depth-dependent Brunt-Väisälä frequency,  $N = N(z)$ . The gradient term  $\nabla\mathbf{U}$  in (3.3) leads to the occurrence of critical layers and is also responsible for wave capture effects (see Section 3.3.2).

Writing the dispersion relation for the frequency of encounter as

$$\omega_{enc} = \Omega_{enc}(\mathbf{K}, \mathbf{X}, t) = \Omega(\mathbf{K}, z) + \mathbf{K} \cdot \mathbf{U}(\mathbf{X}, t) \quad (3.4)$$

we have, according to WKB theory, for the rate of change of frequencies along the ray

$$\begin{aligned} \dot{\omega}_{enc} &= \partial_t\Omega_{enc} = \partial_t\Omega + \mathbf{K} \cdot \partial_t\mathbf{U} \\ \dot{\omega} &= \partial_t\Omega + \mathbf{U} \cdot \partial_{\mathbf{X}}\Omega - \mathbf{V} \cdot (\mathbf{K} \cdot \partial_{\mathbf{X}}\mathbf{U}) \end{aligned} \quad (3.5)$$

Note that  $\mathbf{K}$  contracts with  $\mathbf{U}$  and  $\mathbf{V}$  contracts with  $\partial_{\mathbf{X}}$  in this expression. These frequency relations are consistent with  $\omega = \omega_{enc} - \mathbf{K} \cdot \mathbf{U}$  as integral of the motion along the ray.

If the background medium is time dependent (slow in the WKB sense), resulting in a time-dependent  $\Omega(\mathbf{K}, \mathbf{X}, t)$ , the frequency of encounter changes as given by

(3.5). The wave energy  $E \sim |a|^2$  is then not conserved, but wave action  $A(\mathbf{X}, t) = E(\mathbf{X}, t)/\omega$  (energy over *intrinsic* frequency) is an adiabatic invariant (Landau and Lifshitz 1982; Bretherton and Garrett 1968; Whitham 1970),

$$\partial_t A + \nabla_{\mathbf{X}} \cdot (\dot{\mathbf{X}} A) = 0 \tag{3.6}$$

This property is fundamental for the radiation balance discussed further below.

In a realistic geophysical situation, the wave field is more likely described by a superposition of a great number of wave packets, each localized in physical space and having a dominant wave vector, frequency, and amplitude, which slowly change as a consequence of propagation, refraction, and reflection according to the above ray equations. When two wave packets occupy the same volume, they might interact resonantly for a short finite time and build up a third wave component. This is the process of wave–wave interactions. Wave packets may interact with background fields, e.g. the mean flow, in which they propagate, and new packets may be introduced in the wave ensemble by forcing mechanisms to be discussed in later sections. Instead of using the energy or action of single waves, we describe such a wave field by its energy (power) spectrum<sup>2</sup>  $\mathcal{E}(\mathbf{K}, \mathbf{X}, t) = \omega \mathcal{A}(\mathbf{K}, \mathbf{X}, t)$ , defined such that the integral over wavenumbers yields the local energy density  $E(\mathbf{X}, t)$ . Because the action spectrum is now written as function of  $\mathbf{K}$  in addition to previous independent variables  $\mathbf{X}$  and  $t$ , and the wave vector is also slowly changing, the action conservation reads for the random wave field (Hasselmann 1968)

$$\partial_t \mathcal{A} + \nabla_{\mathbf{X}} \cdot (\dot{\mathbf{X}} \mathcal{A}) + \nabla_{\mathbf{K}} \cdot (\dot{\mathbf{K}} \mathcal{A}) = \mathcal{S} \tag{3.7}$$

Here,  $\mathcal{S}$  is a source, not yet considered in (3.6), representing all processes that may lead to a change of the action spectrum, except for the propagation and refraction processes which are explicitly accounted for on the left-hand side. The vertical energy flux  $\mathbf{F} = \dot{z} \mathcal{E}$  must be specified at the top and bottom boundaries, assuming for simplicity that these are horizontal surfaces. At the surface

$$\mathbf{F}(\mathbf{k}, m) + \mathbf{F}(\mathbf{k}, -m) = \Phi_{surf}(\mathbf{k}, m) \tag{3.8}$$

must hold, and similarly for the bottom with a net flux  $\Phi_{bot}(\mathbf{k}, m)$ . The condition accounts for reflection, in which a wave with vertical wavenumber  $m$  is reflected into one with  $-m$ , and an energy source  $\Phi_{surf}(\mathbf{k}, m)$  by a wave-maker situated at the surface as, e.g. wind stress fluctuations, or tidal conversion at the bottom in case of  $\Phi_{bot}(\mathbf{k}, m)$ .

Application of the radiative transfer will be done in wavenumber coordinates different from the Cartesian ones  $(\mathbf{k}, m)$ . This is because dominant forcing functions are more easily embedded in frequency space, e.g. tidal forcing and near-inertial wave radiation. Also, directional spreading of horizontal wavenumbers is more easily

---

<sup>2</sup> $\mathcal{E}(\mathbf{K}, \mathbf{X}, t) d^3 K$  is the wave energy (density in physical space) in a small wavenumber volume  $d^3 K$  at  $\mathbf{K}$  at the position  $\mathbf{X}$  at time  $t$ .

formulated in angular coordinates. We therefore transform the radiation balance (3.7) into more convenient coordinates. For the balance of  $\tilde{\mathcal{E}} = \tilde{\mathcal{E}}(m, \omega, \phi)$ , we find

$$\partial_r \tilde{\mathcal{E}} + \nabla \cdot \dot{\mathbf{x}} \tilde{\mathcal{E}} + \partial_z \dot{z} \tilde{\mathcal{E}} + \partial_\omega \dot{\omega} \tilde{\mathcal{E}} + \partial_m \dot{m} \tilde{\mathcal{E}} + \partial_\phi \dot{\phi} \tilde{\mathcal{E}} = \omega \tilde{\mathcal{S}} + \dot{\omega} \frac{\tilde{\mathcal{E}}}{\omega} \quad (3.9)$$

Here,  $\dot{\omega}$  is the change of intrinsic frequency along the ray, given by (3.5). The term  $\dot{\omega} \tilde{\mathcal{E}}/\omega$  contains the energy exchange between the waves and the mean flow. We abandon the tilde in the further discussions.

The knowledge about the structure and importance of the oceanic internal wave field is strongly based on experimental evidence of the wave motion. Amplitudes of internal gravity waves are remarkably large, of the order of 10 m (occasionally, they may be an order of magnitude larger), and current speeds are typically 5 cm/s. The wave motion is therefore not difficult to observe; in fact, it is the dominant signal in many oceanic measurements. The first attempt to provide a unified picture of the internal wave field was made by Garrett and Munk (1972) who synthesized a model of the complete wavenumber–frequency spectrum (GM model) of the motion in the deep ocean on the basis of linear theory and the available observations by horizontally or vertically separated moored instruments or dropped sondes. Except for inertial internal waves and baroclinic internal tides, this model is believed to reflect the spectral features of the internal wave climate in the deep ocean and to possess a certain global validity. Most data were in good agreement with the GM model or could be incorporated by slight modifications (Garrett and Munk 1975; Cairns and Williams 1976; Müller et al. 1978; Munk 1981). In a broad-brush view, the GM spectrum is characterized by a  $\omega^{-2}$  decay of energy power in frequency space with a minor peak at  $\omega = f$ , and a  $m^{-2}$  decay in vertical wavenumber space with a roll-off at  $m = m_*$  to a plateau at low wavenumbers; see Figure 3.3. The wavenumber  $m_*$  of the roll-off is referred to as the bandwidth of the spectrum. Note that GM is horizontally isotropic, vertically symmetric, and of the factorized form  $\mathcal{E}(m, \omega, \phi, z) = E(z)A(|m|)B(\omega)/2\pi$ .

Atmospheric gravity wave spectra are reviewed by Fritts and Alexander (2003), and a working base for our purpose of constructing an atmospheric IDEMIX model is presented in Section 3.2.2.2. The general functional class considered for the spectrum is in fact very similar to GM except for a distinct azimuthal distribution of wave propagation directions,  $\mathcal{E}(m, \omega, \phi, z) = E(z)A(|m|)B(\omega)\Phi(\phi)$ . The power laws in frequency and vertical wavenumber are different from GM and seen as not as universal as the oceanic counterpart. The energy level  $E(z)$  and peak (or roll-off) wavenumber  $m_*$  are not following WKB scaling as GM does. Also, as Fritts and Alexander (2003) emphasize, this canonical spectrum does not capture the true complexity of the gravity wave field in altitude and does not account for considerable variability. To a certain degree, this drawback applies as well to GM.

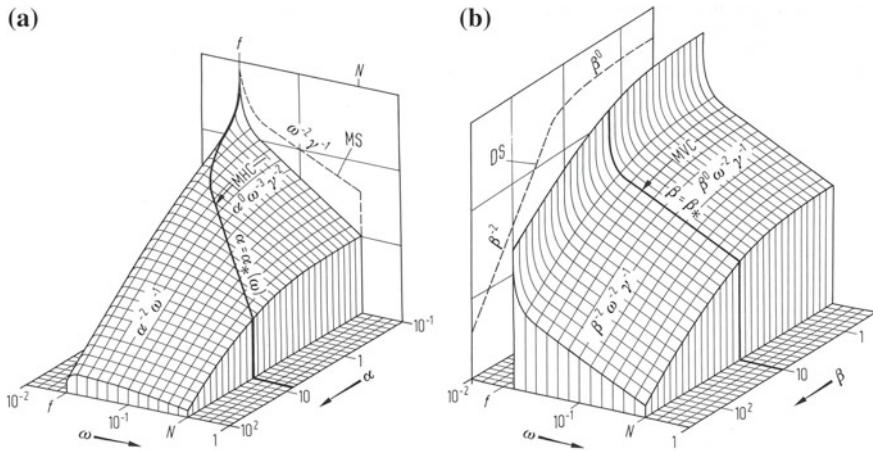


**Fig. 3.3** GM76 model, displayed in (a) as  $\mathcal{E}(k, \omega)$  and in (b) as  $\mathcal{E}(m, \omega)$ . The coordinates are plotted logarithmically so that plane surfaces represent power laws, some of which are indicated in the graphs. The partially integrated forms MS and DS of the moored and dropped spectra, respectively, are displayed as respective projections, and the moored coherences MHC and MVC are related to the corresponding bandwidths, as indicated. All quantities are normalized with reference to the scale  $b$  and  $N_0$  of the Brunt-Väisälä frequency profile  $N(z) = N_0 e^{z/b}$ . In the figure, the notation  $\alpha = k$ ,  $\beta = m$ , and  $\gamma = (1 - f^2/\omega^2)^{1/2}$  is used. After Garrett and Munk (1975), Olbers (1986)

### 3.2 The IDEMIX Model

Müller and Natarov (2003) suggested to base a model for the propagation and dissipation of internal waves on the radiative transfer equation (3.7) of weakly interacting waves in the 6-dimensional phase space. However, theoretical, practical, and numerical limits hamper the realization of such a comprehensive model. Olbers and Eden (2013) discussed a drastic simplification of the concept which they called IDEMIX (Internal wave Dissipation, Energy and Mixing). Instead of resolving the detailed wave spectrum as suggested by Müller and Natarov (2003), they integrate the spectrum in wavenumber and frequency domain, leading to conservation equations for integral energy compartments in physical space. These equations can be closed with a few simple but reasonable parameterizations. IDEMIX describes the generation, interaction, propagation, and dissipation of the internal gravity wave field and can be used in ocean general circulation models to account for vertical mixing (and friction) in the interior of the ocean. In its simplest version, IDEMIX consists of two compartments of interacting up- and downward propagating waves (Olbers and Eden 2013). In a more complex version, low vertical mode compartments at near-inertial frequencies and frequencies of tidal constituents are added which also account for horizontally anisotropic wave propagation (Eden and Olbers 2014). For some more details, we refer to Section 3.2.1. Eden et al. (2014) demonstrate how an energetically consistent ocean model can be constructed connecting IDEMIX with other



energy-based parameterizations for the unresolved dynamical regimes of mesoscale eddies and small-scale turbulence. IDEMIX is central to the concept of an energetically consistent ocean model, since it enables to link all sources and sinks of internal wave energy, and furthermore all parameterized forms of energy in an ocean model without spurious sources and sinks of energy.

### 3.2.1 Details of the Oceanic IDEMIX

Both the simple and extended versions of IDEMIX are based on the radiative transfer equation (3.9) and the boundary condition (3.8) which describe the evolution in time of the energy spectrum  $\mathcal{E}(m, \omega, \phi, \mathbf{x}, z, t)$  of an ensemble of weakly interacting gravity waves in wavenumber and physical space. Using the 6-dimensional space  $(m, \omega, \phi, \mathbf{x}, z)$  is too difficult, and integrated energy compartments are thus considered instead. In the simple version of IDEMIX by Olbers and Eden (2013),  $\mathcal{E}$  is integrated over frequency  $\omega$ , azimuth  $\phi$ , and over vertical wavenumber  $m$ , but separately for positive  $m$  (yields  $E^-$ , downward propagating waves) and negative  $m$  (yields  $E^+$ , upward propagating waves). Defining total energy  $E = E^+ + E^-$  and energy asymmetry  $\Delta E = E^+ - E^-$ , the projection of (3.7) leads to

$$\begin{aligned} \partial_t E + \partial_z c_0 \Delta E &= -F_{diss} = -\mu E^2 \\ \partial_t \Delta E + \partial_z c_0 E &= F_{ww} = -\Delta E / \tau_v \end{aligned} \quad (3.10)$$

This applies to the simplest IDEMIX model where horizontal homogeneity is assumed. The crosswise form of the vertical energy fluxes in (3.10) derives from the vertical group velocity  $\dot{z} = \pm c$  of up- and downward waves being opposed to the vertical wavenumber  $m$ . However, a parameterization of the integrated group velocity is needed, and this is done in a typical way for parameters in IDEMIX energy balances: here, the mean vertical propagation with group speed  $c_0$  is calculated analytically by assuming a spectrum of the gravity wave field of fixed shape but unknown amplitude  $E$ , the factorized GM76 spectrum (which may vary with  $E$  in space and time). The form of the energy balances is thus exact, but the group velocity  $c_0$  (modulus) is that of a related GM spectrum. IDEMIX consequently assumes that the actual wave spectrum is always close to the GM spectrum with respect to the shape; the unknown energy is then given by  $E^\pm$  or  $E$  and  $\Delta E$  and governed by (3.10).

Surface and bottom reflections lead to a flux from  $E^\pm$  to  $E^\mp$ , respectively, and forcing by tides and near-inertial pumping is added as a surface and bottom flux  $\sim \Delta E$  into the total wave energy  $E$ , resulting from the integration of (3.8). Wave-wave interactions in the simple IDEMIX version are parameterized as damping of the differences of up- and downward propagating waves with a timescale of a few days, leading to the relaxation term  $F_{ww}$  in the asymmetry balance of (3.10). This simple closure is supported by the observation of a nearly symmetric wave field in  $m$  (as the GM spectrum) and the evaluation of the wave-wave interactions for



slightly perturbed GM spectra (McComas 1977). There is no corresponding term in the balance of total energy since wave–wave interactions conserve energy. The closure for the dissipation of gravity waves in (3.10) by the term  $F_{diss} = \mu E^2$  follows the method of finestructure estimates of dissipation rates (Gregg 1989; Kunze and Smith 2004) and is given by a quadratic functional in the total wave energy  $E$ , as found by Olbers (1976), McComas and Müller (1981) from the scattering integral of resonant triad interactions. The parameter  $\mu$  is a known function of  $N$ ,  $f$ , and the GM bandwidth  $m_*$ .

The simple IDEMIX version can be extended to horizontal inhomogeneity conditions but cannot treat well lateral propagation of waves. This issue is resolved in the extended IDEMIX version by Eden and Olbers (2014), where low vertical mode energy compartments  $E_n$  at fixed frequency  $\omega_n$  (e.g. tidal frequency) are separated from the rest (the wave continuum) and which resolve horizontal wave propagation. The  $E_n$  are accordingly governed by a corresponding radiative transfer equation

$$\partial_t E_n + \nabla \cdot \mathbf{c}_g E_n + \partial_\phi \dot{\phi} E_n = W_n + T_n \quad (3.11)$$

where  $\mathbf{c}_g$  denotes the lateral group velocity at  $\omega_n$ , and  $\dot{\phi}$  denotes the refraction of the wavenumber angle  $\phi$  with  $\mathbf{k} = k(\cos \phi, \sin \phi)$ . The  $E_n$  are functions of  $\mathbf{x}$  and  $\phi$  (and time) and are chosen as tides  $M_2$ ,  $S_2$  or local near-inertial waves. They are represented by vertically integrated low vertical modes, while all other frequencies and higher vertical modes are still contained in the vertically resolved wave continuum  $E^+$  and  $E^-$ .

Equation (3.11) describes the lateral propagation and refraction of low-mode baroclinic tidal or near-inertial energy compartments, the scattering into the wave continuum by rough topography by the term  $T_n$ , and the wave–wave interaction with the continuum by the term  $W_n$ , which were derived analytically by Eden and Olbers (2014). They show up with opposite signs in the conservation equation for  $E = E^+ + E^-$ . Tidal forcing enters in the extended version of IDEMIX partly as a bottom flux for the wave continuum as in the simple IDEMIX version, but also in the energy compartment of the respective tidal constituent where it will laterally propagate over considerable distances before it is transferred to the wave continuum and to dissipation. Both the simple and extended versions of IDEMIX are available as stand-alone versions with prescribed stratification and forcing without feedback on the circulation, and coupled to a general circulation model (<https://wiki.zmaw.de/ifm/TO/pyOM2>).

The link from the wave energy balance to mixing is as follows. Knowledge of the wave energy  $E$  enables us to compute the wave dissipation term  $F_{diss} = \mu E^2$  which is a source of turbulent kinetic energy (TKE). Assuming steady state and a few other simplifications, the TKE balance reads (Osborn and Cox 1972)

$$F_{diss} + \overline{b'w'} - \varepsilon = 0 \quad (3.12)$$

Here,  $\overline{b'w'}$  denotes the vertical turbulent buoyancy flux, i.e. the exchange with potential energy, and  $\varepsilon$  the dissipation rate of TKE by molecular friction, i.e. the exchange

with internal energy ('heat'). Assuming a conventional downgradient turbulent buoyancy flux  $\overline{b'w'} = -K_\rho N^2$ , where  $K_\rho$  denotes a vertical diffusivity, and a constant mixing efficiency  $\delta = K_\rho N^2 / \varepsilon$  (usually taken equal 0.2), the diffusivity  $K_\rho$  can be computed from the wave energy  $E$  and given  $\delta$ . More elaborate coupling of TKE and  $E$  is considered in Eden et al. (2014).

### 3.2.2 *The IDEMIX Concept Applied to Atmospheric Gravity Waves*

IDEMIX is not yet realized for atmospheric internal gravity waves. We describe here how an atmospheric IDEMIX can be built. Unlike the ocean case where parameterization of mixing is a first goal, the atmospheric IDEMIX should aim at parameterization of wave drag, i.e. the wave-induced Reynolds stress.

We restrict ourselves to the single-column approximation (i.e. we assume a horizontally homogeneous background flow at each geographical location, which is analogous to the plane-parallel approximation in radiative transfer computations) such that the coordinate dependence is reduced to that on height  $z$ . Furthermore, we assume gravity wave propagation only in particular azimuthal directions. In the actual gravity wave parameterization, we then add up the contributions from 4 or 8 equally distributed azimuths, denoted by the index  $j$ . Note that these approximations are made as well in any conventional gravity wave scheme used in climate models. Regarding the dependence on the wavenumber vector in horizontal and vertical directions, we express the spectral energy density with regard to the horizontal wavenumber  $k$  in terms of the intrinsic frequency,<sup>3</sup> denoted as  $\omega$ . The total spectral energy is given by  $\mathcal{E}(m, \omega, \phi, z, t) = \sum_j \mathcal{E}_j(m, \omega, z, t) \delta(\phi - \phi_j)$ . The radiative transfer equation

$$\partial_t \mathcal{E}_j + \partial_z (\dot{z} \mathcal{E}_j) + \partial_m (\dot{m} \mathcal{E}_j) + \partial_\omega (\dot{\omega} \mathcal{E}_j) = S_j + \dot{\omega} \mathcal{E}_j / \omega - D m^2 \mathcal{E}_j \quad (3.13)$$

for the wave energy compartment for the azimuth direction  $j$  is derived from (3.9) after integration over the azimuth angle. Our sign convention is such that  $\omega > 0$  and  $m < 0$  for upward group propagation (downward phase propagation), as before for the oceanic case. In (3.13),  $D = D(z, t)$  denotes a vertical diffusion coefficient which describes damping due to wave breaking. This coefficient must be computed according to some dynamic stability criterion and should in principle also include the diffusion coefficient computed by the vertical diffusion scheme of the model (e.g. the boundary layer diffusion will damp orographic gravity waves). Furthermore,  $S_j = S_j(m, \omega, z, t)$  is a source function that needs to be specified in order to describe the various generation mechanisms of atmospheric gravity waves such as flow over a rough surface, convection, frontal activity, and secondary gravity waves. Wave-wave

---

<sup>3</sup>Conventional parameterization schemes often assume a fixed  $k$  for the assumed gravity wave spectrum.

interactions would also add to  $S_j$ , but are not further discussed here since they play a less dominant role compared to the ocean. The other terms in (3.13) describe wave propagation, wave refraction, and interactions (reversible and irreversible) with the mean flow.

For the ocean case, energy compartments of up- and downward propagating waves are considered. This is important because of the nearly vertical symmetry of the wave field in the ocean, but less so for the atmosphere since surface reflection and strong wave–wave interactions, which lead to the symmetry, are missing. Reflection at the top is entirely absent. We will therefore dispense with this differentiation in compartments of up- and downward propagating waves for the atmosphere. We propose to use four directional compartments as a starting point. Conventional gravity wave schemes for atmosphere models often use 8 azimuthal directions.

### 3.2.2.1 Wave–Mean Flow Interaction and Energy Conservation

Regarding the effects of the parameterized gravity wave spectrum on the mean flow, we resort to the general theoretical framework of the two-way Reynolds average approach to filter out small-scale turbulence and mesoscale gravity waves as presented in Becker (2004) and Becker and McLandress (2009). A more detailed discussion can also be found in Shaw and Shepherd (2009). For a prognostic gravity wave scheme as envisioned in our case, the following framework applies. The rate of change of mean momentum and energy by the wave-induced stress is

$$(\rho \partial_t \mathbf{v})_{GW} = -\partial_z \mathbf{F} \tag{3.14}$$

$$(\rho c_p \partial_t T)_{GW} = -(\partial_z F_p + \mathbf{F} \cdot \partial_z \mathbf{v}) - \partial_t e_{GW} \tag{3.15}$$

Here,  $\mathbf{v}$  denotes the horizontal wind vector of the mean flow, and hence, the left-hand side of (3.14) simply describes the familiar gravity drag. The in situ air temperature is denoted by  $T$ , and the direct heating that accompanies the gravity wave drag is given by the right-hand side of (3.15), where the first term is the so-called energy deposition (e.g. Hines 1997). The energy deposition involves both the vertical flux of horizontal momentum,  $\mathbf{F}$ , and the pressure flux,  $F_p$ , induced by the wave field. The second term is the tendency of the total energy<sup>4</sup> of the gravity wave field, denoted as  $e_{GW}$ . This energy

$$e_{GW}(z, t) = \sum_j \int_{-\infty}^{-m_0} dm \int_{\omega_0}^{\omega_1} d\omega \mathcal{E}_j(m, \omega, z, t) \tag{3.16}$$

is obtained by integrating (3.13) over wavenumber and frequency and by summation over all azimuths. Here,  $m_0$  defines a minimum absolute vertical wavenumber,  $\omega_0$  a

---

<sup>4</sup>This direct heating term vanishes for a conventional parameterization due to the assumption of stationary wave energy.

minimum intrinsic frequency that is of the order of the Coriolis parameter at middle latitudes, and  $\omega_1$  a maximum intrinsic frequency that is of the order of the background buoyancy frequency  $N$ .

Energy conservation is trivially fulfilled since  $F_p$  and  $\mathbf{v}$  vanish at the surface,  $z = z_s$ , and since  $\mathbf{F}$  and  $F_p$  vanish for  $z \rightarrow \infty$ . Hence,

$$\int_{z_s}^{\infty} dz \partial_t e_{GW} + \int_{z_s}^{\infty} dz \mathbf{v} \cdot (\rho \partial_t \mathbf{v})_{GW} + \int_{z_s}^{\infty} dz (\rho c_p \partial_t T)_{GW} \equiv 0 \quad (3.17)$$

The momentum flux and pressure flux are obtained by using the polarization relations for gravity waves having vertical wavelengths not larger than the scale height, yielding

$$\mathbf{F}(z, t) = \sum_j F_j (\cos \phi_j \mathbf{e}_x + \sin \phi_j \mathbf{e}_y) \quad (3.18)$$

with

$$F_j(z, t) = \int_{-\infty}^{-m_0} dm \int_{\omega_0}^{\omega_1} d\omega \frac{\omega}{N} \mathcal{E}_j(m, \omega, z, t)$$

$$F_p(z, t) = \sum_j \int_{m_0}^{\infty} dm \int_{\omega_0}^{\omega_1} d\omega \frac{\omega}{m} \mathcal{E}_j(m, \omega, z, t) \quad (3.19)$$

Here,  $\phi_j$  is the angle of the azimuthal direction  $j$  with the unit vector in eastward direction denoted as  $\mathbf{e}_x$ , while  $\mathbf{e}_y$  is the unit vector in northward direction. In these expressions, the mid-frequency approximation was made which can, however, be relaxed as for the oceanic IDEMIX version.

### 3.2.2.2 Factorization of the Spectrum and Prognostic Equations

Since the treatment of (3.13) in the 3-dimensional space  $(z, m, \omega)$  will be computationally too expensive, we follow the IDEMIX concept and assume a simple factorization of the wave spectrum with unknown amplitude  $E_j(z, t)$ . Having  $\mathcal{E}_j(z, t, m, \omega)$  in such a form, the integrals over  $m$  and  $\omega$  for the fluxes (3.19) in the model equations (3.14) and (3.15) are readily calculated as functionals of  $E_j(z, t)$ . The assumption of a factorized wave spectrum with unknown amplitude is key to the IDEMIX concept which we also use here, but we also allow for variations of the shape parameters.

While a generic spectral shape is observed in the ocean with only rare exceptions, this is not expected for the atmosphere. We therefore attempt to introduce additional prognostic equations to characterize the spectral shape. This concept was originally

introduced by Hasselmann et al. (1973) for the simulation of the energetics of surface wind waves. In the atmospheric case, the generalized Desaubies spectrum according to Fritts and VanZandt (1993) has proven to work well in advanced gravity wave schemes using the conventional framework (Scinocca 2003). Here, we apply the Desaubies spectrum (Desaubies 1976) (this actually is a derivative of GM; see also Müller et al. 1978) for each azimuthal direction as:

$$\mathcal{E}_j(m, \omega, z, t) = E_j(z, t) n(\omega_0, m_j^*(z, t), q, r, s) \left(\frac{\omega_0}{\omega}\right)^q \frac{(m/m_j^*(z, t))^s}{1 + (m/m_j^*(z, t))^{r+s}} \quad (3.20)$$

Like in IDEMIX,  $E_j(z, t)$  is the total energy contained in the spectrum at  $(z, t)$ ; i.e.  $n$  is a normalization factor such that  $E_j = \int d\omega \int dm \mathcal{E}_j$ . The shape of the spectrum regarding its  $m$ -dependence is allowed to vary with height and time via the parameter  $m_j^*(z, t)$ . The exponent  $q$  used in (3.20) can be chosen within  $1 \leq q \leq 5/3$ , while typical values for  $s$  and  $r$  are 1 and 3, respectively. As a starting point for the new parameterization, we set  $q = 1$ ,  $s = 1$ , and  $r = 3$ . For large  $m$ , the spectrum is then proportional to  $m^{-3}$ . Such a behaviour is consistent with the scaling laws of stratified turbulence.<sup>5</sup>

To compute the temporal evolution of  $E_j(z, t)$  and  $m_j^*(z, t)$ , we have to solve (3.13) for each azimuth. To this end, we have to compute  $\dot{z}$  and  $\dot{\omega}$  from the dispersion relation. For the most simple case of mid-frequency gravity waves with upward group propagation (i.e. for  $m < 0$ ), we get  $\dot{z} = -\omega/m$ ,  $\dot{m}_j = N^{-1}\omega (m \partial_z u_j + \partial_z N)$  and  $\dot{\omega}_j = -\omega^2 N^{-1} \partial_z u_j$ , where  $u_j$  is the projection of  $\mathbf{v}$  into the direction of  $\phi_j$ . Furthermore, we have to specify the diffusion coefficient and some source functions. In IDEMIX, the resulting radiative transfer equation is then integrated over  $m$  and  $\omega$  to obtain a prognostic equation for just the amplitude of the spectrum, i.e. for  $E_j(z, t)$ .

To allow, however, for variations of the spectral shape with altitude and time, we use another method to solve (3.13). We propose to apply the Gaussian variation principle in order to determine  $\partial_t E_j(z, t)$  and  $\partial_t m_j^*(z, t)$  from the functional derivatives

$$\frac{\delta \chi_j^2(z, t)}{\delta (\partial_t E_j(z, t))} = 0, \quad \frac{\delta \chi_j^2(z, t)}{\delta (\partial_t m_j^*(z, t))} = 0 \quad (3.21)$$

that are obtained from requiring that

$$\chi_j^2(z, t) = \int_{-\infty}^{-m_0} dm \int_{\omega_0}^{\omega_1} d\omega \left[ \partial_t \mathcal{E}_j + \partial_z (\dot{z} \mathcal{E}) + \partial_m (\dot{m}_j \mathcal{E}) + \partial_\omega (\dot{\omega}_j \mathcal{E}) - S_j - \dot{\omega}_j \mathcal{E}_j / \omega + D m^2 \mathcal{E}_j \right]^2 \quad (3.22)$$

<sup>5</sup>The aspect ratio for stratified turbulence,  $k \propto m^3$ , converts a spectral energy density proportional to  $m^{-3}$  into a  $k^{-5/3}$ -spectrum with respect to the horizontal wavenumber.

is minimum. The procedure is straightforward. All integrals in (3.22) for  $m$  and  $\omega$  can be solved analytically.

### 3.2.2.3 Dissipation and Forcing

A particular and important aspect of the project is to set up a proper parameterization of the diffusion coefficient,  $D(z, t)$ , and the source function  $S_j(m, \omega, z, t)$  to force gravity waves. Regarding the diffusion, we plan to rely on the saturation assumption of Lindzen (1981) which has proven to work equally well for non-orographic and orographic gravity waves (see the model description in Garcia et al. 2007). This has, however, to be further specified for the present entirely new framework for an atmospheric gravity wave scheme. Also note that, like in the generalized Doppler spread parameterization of Becker and McLandress (2009), the diffusion coefficient should be the same for the entire gravity wave field.

While wave–wave interactions are of importance in the oceanic case, this appears less so for the atmosphere. Wave–wave interactions will thus be neglected in the first phase. The dissipation in the oceanic case is inferred from the flux in wavenumber space due to wave–wave interactions to large vertical wavenumbers and is a quadratic functional of the total wave energy (Olbers 1976; Müller et al. 1986), which is also used for observational estimates of dissipation rates (Gregg 1989; Kunze and Smith 2004). It remains to be seen how this process relates to the aforementioned non-linear wave-breaking theories and whether it can eventually be incorporated in the new atmospheric gravity wave scheme.

Regarding the source function, we plan to use specifications for gravity wave generation by orography, frontal activity, and convection that have proven to work well in conventional schemes used in global climate models. We will take advantage of the specification of orographic sources as proposed by McFarlane (1987) and use gravity wave sources due to frontal activity and convection as outlined by Charron and Manzini (2002) and Richter et al. (2010).

## 3.3 Oceanic Processes in Present and Future IDEMIX

Internal gravity waves have a major share of the energy contained in oceanic motions (e.g. Wunsch and Ferrari 2004). When they break by shear or gravitational instability, they feed their energy to small-scale turbulence in the interior of the ocean and thus contribute to density mixing. This process, transferring wave energy to large-scale potential energy, becomes an important part of the oceanic energy cycle. It is furthermore thought to be an important driver of the ocean circulation (e.g. Wunsch and Ferrari 2004; Kunze and Smith 2004).

The part of the gravity wave field which is prone to break is by far unresolved by ocean model components of climate models, since a lateral and vertical resolution of less than 100 and 10 m, respectively, is required. Consistent parameterizations to

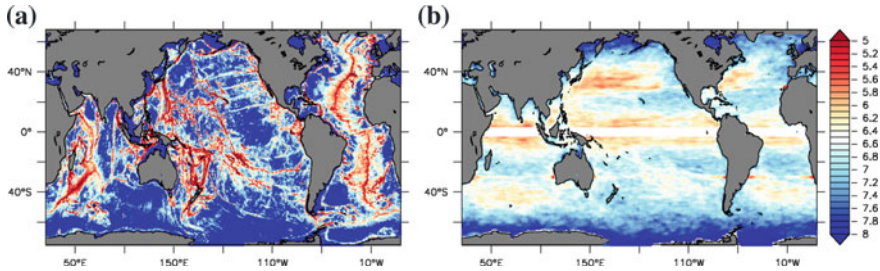


**Fig. 3.4** (a) Tidal forcing and (b) near-inertial wave forcing in  $\log_{10} F / [\text{m}^3 \text{s}^{-3}]$

include the effects of wave breaking have been missing for a long time. A varying diffusivity was introduced for the ocean interior by Bryan and Lewis (1979) with a prescribed depth function and, among others, by Cummins et al. (1990) with a dependence on the stability frequency. The energy source for mixing was not specified in these and other early approaches although the vertical diffusivity was supposed to parameterize the effect of breaking internal waves. Jayne and St. Laurent (2001) suggested to link the conversion of barotropic tidal energy into internal waves as simulated by a barotropic tidal model to a profile of vertical diffusivity adapted to observations. However, the lateral spreading of baroclinic tides and the effect of the other sources of gravity waves are left unconsidered, and the parameterization remains energetically inconsistent. The recently developed IDEMIX concept (Olbers and Eden 2013; Eden and Olbers 2014), on the other hand, implements this spreading and treats gravity wave sources in an energetically consistent way. For details, see Section 3.2.1.

Prominent forcing mechanisms of internal waves occur very localized in the frequency domain. Near-inertial waves with frequencies slightly above the local Coriolis frequency are excited by wind stress fluctuations at the surface (Alford 2001; Rimac et al. 2013) and can propagate over large distances in horizontal direction, while slowly propagating down into the interior ocean (Garrett 2001). A further monochromatic source is related to the scattering of the barotropic tide at topography, predominantly at the continental shelf, the mid-ocean ridges but also at the more random-type small-scale roughness of the seafloor (Nycander 2005). The flux from the barotropic tide into the internal wave field occurs at the ocean bottom, shown in Figure 3.4(a). The flux from radiation of near-inertial waves out of the surface mixed layer is depicted in Figure 3.4(b). These fluxes are currently the main drivers implemented in the IDEMIX versions.

Several other generation processes have been discussed (see, e.g., Thorpe 1975; Müller and Olbers 1975; Olbers 1983, 1986; Polzin and Lvov 2011) occurring over a broad range of frequencies, e.g. dissipation of mesoscale eddies by spontaneous wave emission or other processes (Ford et al. 2000; Molemaker et al. 2010; Tandon and Garrett 1996; Eden and Greatbatch 2008a; Brüggemann and Eden 2015), resonantly interacting surface gravity waves (Olbers and Herterich 1979; Olbers and Eden 2016), the generation of lee waves by large-scale currents or mesoscale eddies flowing over



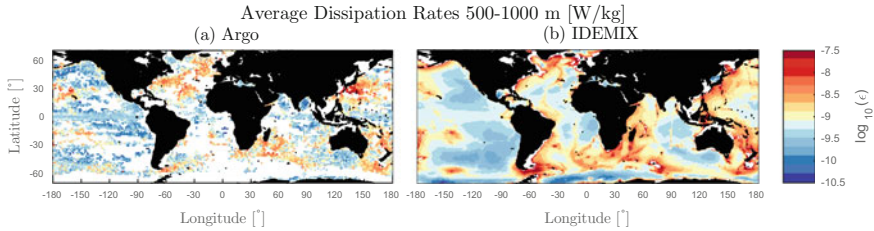


**Fig. 3.5** Validation of the simple IDEMIX version: (a) observational estimate of the dissipation of gravity wave energy calculated from density profiles of ARGO floats following Whalen et al. (2012) averaged between 500 and 1000 m. (b) Same as (a) but simulated by IDEMIX in a fully coupled mode. From Pollmann et al. (2017)

topography (Nikurashin and Ferrari 2011), and wave–mean flow interaction (Müller 1976; Polzin 2008). There are also indications that mixed-layer turbulence generates waves close to the local stability frequency below the mixed layer (Bell 1978).

Both IDEMIX versions show agreement with observational estimates in first diagnostics, but also biases: Figure 3.5 shows that magnitude and lateral pattern of the simulated dissipation rates of internal waves in the simple IDEMIX version agree with observational estimates (more details in Section 3.3.5). It turns out that the dissipation of mesoscale eddy energy is important for the maxima in dissipation rates seen in the western boundary currents and the Antarctic Circumpolar Current (ACC). Without the eddy dissipation, some of these maxima are not simulated (not shown). In the Southern Ocean, however, IDEMIX simulates too much dissipation within the ACC and thus too large diffusivities (as shown in Eden et al. 2014), when all eddy energy is dissipated locally and injected into the wave field as assumed in the mesoscale eddy closure by Eden and Greatbatch (2008b). This points towards the need to better understand the dissipation of mesoscale eddy energy and its relation to the internal wave field. More details are given in Section 3.3.1.

When waves are propagating in a vertically sheared mean flow, they exchange energy with the mean flow and even can break due to critical layer absorption or wave capture. The former effect is also called gravity wave drag in the atmospheric literature (see Section 3.2.2.1), where it is of importance for the dynamics of the upper atmosphere. The direction of the energy exchange can be from the mean flow to the waves or vice versa. When waves break in a critical layer, on the other hand, their energy is transferred to small-scale turbulence. In Section 3.2.2.1, we propose an extension of IDEMIX to incorporate the energy exchange with the mean flow for the atmospheric case. The effect on the mean flow figures in this concept as a divergence of a vertical eddy momentum flux due to wave activity in the residual momentum equation, similar to vertical friction, but can accelerate and decelerate the mean flow. It can be shown that the energy transfer between waves and large-scale mean flow is present in the ocean, but amounts to only a fraction of, e.g. the energy exchange between mean flow and mesoscale eddies (see Section 3.3.2). However, the effect of critical layers where waves break and contribute to density mixing has

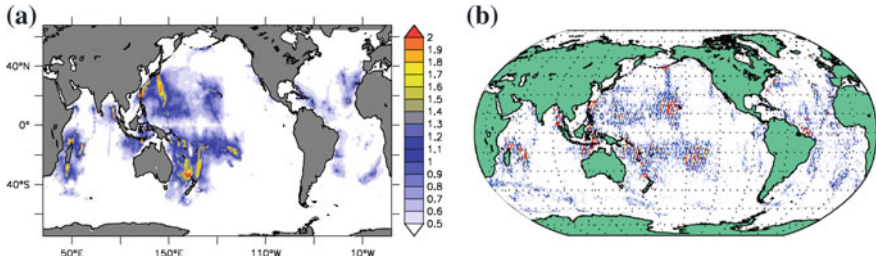


**Fig. 3.6** Validation of the extended IDEMIX version: (a) equivalent surface elevation  $\zeta$  due to the baroclinic  $M_2$  tide in cm simulated by IDEMIX. (b) Observed surface elevation  $\zeta$  in m of  $M_2$  tide taken from Müller et al. (2012) on the same colour scale as in (a). Taken from Eden and Olbers (2014)

not been discussed so far in IDEMIX, although this might be the more important effect in the ocean. Effects similar to critical layers occur when horizontally sheared mean currents are present; the process is called wave capture (see, e.g., Jones 1969; Bühler and McIntyre 2005). This points towards the need to include wave–mean flow interaction and the effect of critical layers and wave capture into IDEMIX. We expand this issue further in Section 3.3.2.

Figure 3.6 shows that the extended version of IDEMIX simulates well the generation of the low-mode  $M_2$  tide and also its propagation but that there are also biases. It remains at the moment unclear whether these differences are due to errors in the observational estimates—the identification of the baroclinic tidal signal in the altimeter data is rather difficult (Dushaw et al. 2011)—but it is clear that IDEMIX also has shortcomings. Most important is the forcing by the barotropic tide, which is taken at the moment for simplicity as isotropic for the wave propagation direction. On the other hand, anisotropic wave generation is most likely responsible for many features seen in the observational estimates, such as the energy maximum between the Aleutian and the Hawaiian Islands which is not reproduced by IDEMIX. This points towards the need to include anisotropic wave generation in IDEMIX and a detailed comparison with observations and direct simulations of baroclinic tides in ocean models. Details are found in Section 3.3.3.

Unlike the internal wave energy generated by near-inertial motions in the mixed layer and the tides which have low frequencies and propagate through the entire water column, internal waves generated by resonant interactions of surface waves are of high frequency (Olbers and Herterich 1979; Olbers and Eden 2016). The same is true for the wave generation by mixed-layer turbulence near the stability frequency (Bell 1978; Polton et al. 2008). Since the stability frequency at larger depth is normally much smaller than within the seasonal thermocline close to the mixed layer or the upper permanent thermocline, waves generated by these processes have shallow turning points and are thus likely to be trapped in the upper ocean. They could contribute to mixing just below the mixed layer. Recent estimates of the global energy transfer from the surface waves to the internal wave field are given by Olbers

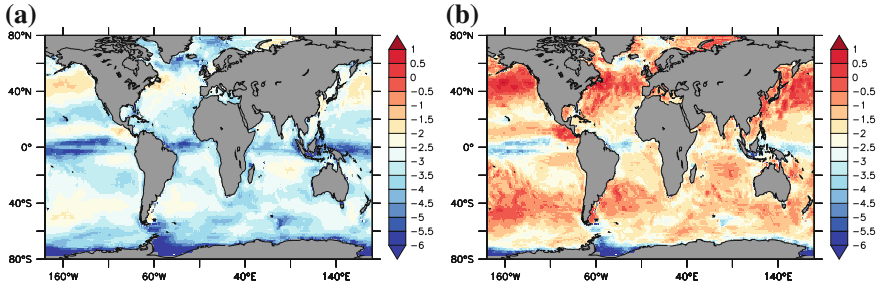


**Fig. 3.7** (a) Mean flux from surface waves to internal waves in  $\log_{10}(\Phi_{tot}/[\text{mW}/\text{m}^2])$  in 2010. (b) Same as (a) but maximum of the year. From Olbers and Eden (2016)

and Eden (2016). Figure 3.7 shows the annual mean total flux and its maximum during the year. The largest fluxes show up in the storm track regions of the oceans, while towards the equator the flux and its maximum almost vanish. The implied dissipation rates are found to reach magnitudes comparable to observational estimates close to the mixed layer, in particular during strong wind events. This points towards the need to include in IDEMIX surface–internal wave interactions and waves generated by mixed-layer turbulence. See Section 3.3.4 for more details.

### 3.3.1 Including Energy Transfers from Mesoscale Eddies to Internal Waves

Dissipation of balanced flow is thought to happen on different routes; lee wave generation, bottom friction, and loss of balance are often considered as important processes. Other processes which have been discussed are topographic inviscid dissipation of balanced flow (Dewar and Hogg 2010), direct generation of unbalanced ageostrophic instabilities (Molemaker et al. 2005), or geostrophic adjustment of balanced flow (Wang and Zhang 2010). Further, wave–mean flow interaction can lead to an energy transfer between the wave field and the vertically sheared mesoscale and large-scale mean flow, a process called gravity wave drag in the atmospheric literature. This ‘drag’, however, can take both directions.

#### 3.3.1.1 Lee Wave Generation

Scott et al. (2011) estimate an energy flux of 0.34 to 0.49 TW as the global transfer of energy by internal lee wave generation of eddies and mean flow over varying topography, while Nikurashin and Ferrari (2011) estimate a lower energy flux of 0.2 TW by the process. However, both numbers are only a fraction of the total eddy energy production: von Storch et al. (2012) report 0.83 TW global eddy energy

production by conversion from mean to eddy available potential energy (baroclinic instability) and additionally a transfer of 0.1 TW from mean to eddy kinetic energy (barotropic instability) in agreement with observational estimates.

Linear theory (Bell 1975) shows that the energy flux into the internal wave field for subcritical topographic slopes is given by

$$F_{lee} = \frac{\rho_0}{4\pi^2} \int_{f^2 < (\mathbf{U} \cdot \mathbf{k})^2 < N^2} d^2k P(\mathbf{k}) \mathbf{U} \cdot \mathbf{k} / |\mathbf{k}| \sqrt{N^2 - (\mathbf{U} \cdot \mathbf{k})^2} \sqrt{(\mathbf{U} \cdot \mathbf{k})^2 - f^2} \quad (3.23)$$

where  $P(\mathbf{k})$  is the topography spectrum,  $\mathbf{U}$  the balanced bottom flow,  $N$  is the stability frequency at the bottom, and  $\mathbf{k}$  the horizontal wave vector. We will implement the effect of lee wave generation using for (3.23) estimates of topographic spectra from Goff and Arbic (2010) and magnitudes of balanced bottom flow from the model of von Storch et al. (2012). To describe the topography spectrum, we use (as in Eden and Olbers 2014) digital maps of geophysical parameters given by Goff and Arbic (2010) for the root mean square topographic height  $h_{rms}$  of abyssal hills and  $\bar{k} = 2\pi/\lambda_n$ , where  $\lambda_n$  is a characteristic width and  $\bar{k}$  a mean wavenumber. These maps are based on estimates of palaeo-spreading rates of the mid-oceanic ridge system and sediment thickness. Specific formulae for  $h_{rms}$  and  $\lambda_n$  and data sources are given in Eden and Olbers (2014). Assuming an isotropic spectrum and a fixed power law for  $P(k) = P_0 k^{1-\mu}$ , it is possible to evaluate the integral in (3.23) for  $|f| \ll N$  analytically as

$$F_{lee} \approx \frac{\rho_0 P_0}{\pi} N |\mathbf{U}|^{5/2} f^{-1/2} \left( \frac{9}{5} - \frac{7}{3} |f/N|^{1/2} + O(f^2/N^2) \right) \quad (3.24)$$

written here for simplicity for the parameter  $\mu = 7/2$ , as suggested by Nikurashin and Ferrari (2011). Note that  $P_0$  relates to  $h_{rms}^2$ , if evaluated for the characteristic range of lee waves  $P_0 = 4h_{rms}^2/\lambda_n \sqrt{|U|/f}$ . We will compute the flux  $F_{lee}$  from the bottom flow  $\mathbf{U}$  of the global eddy-resolving STORM model (von Storch et al. 2012), which provides a map of energy injection due to lee wave generation as lower boundary condition for a stand-alone version of IDEMIX (in addition to the tidal forcing). For IDEMIX coupled to a non-eddy-resolving general circulation model, we will use the mean flow from that model, and in addition the (square root of) EKE from the closure by Eden and Greatbatch (2008b) for  $\mathbf{U}$  in (3.24).

### 3.3.1.2 Bottom Friction

The transfer by bottom friction is likely of similar order of magnitude as the one by lee wave generation: the dissipation of eddy energy by bottom friction was estimated by Arbic et al. (2009) from different model bottom velocities as a global energy transfer ranging between 0.14 and 0.65 TW by a simple quadratic drag law. In the model by von Storch et al. (2012), the global transfer is only 0.12 TW (Brüggemann and Eden

2015). Here, we will assume that bottom friction generates small-scale turbulence in a bottom boundary layer only, without energy transfer to internal waves.

### 3.3.1.3 Loss of Balance

Williams et al. (2008) estimate 1.5 TW energy extracted from quasi-geostrophic flow and transferred into internal gravity waves by Lighthill radiation (Lighthill 1952) based on a laboratory experiment extrapolated to the global ocean. Although their extrapolation is presumably quite crude, the experiment suggests that dissipation by Lighthill radiation might play an important role in the ocean energy cycle. Brüggemann and Eden (2015) find in idealized model experiments of forced-dissipative baroclinic instability that a kinetic energy cascade towards smaller scales is generated for dynamical conditions characterized by a low Richardson number ( $Ri$ ) or large Rossby number ( $Ro$ ), i.e. for ageostrophic conditions, while the familiar inverse energy cascade towards larger scales (and to bottom friction) dominates for  $Ri \gg 1$  or  $Ro \ll 1$ . From a simple fit of the energy transfer towards smaller scales as a function of the local  $Ri$ , Brüggemann and Eden (2015) estimate the fraction of the local baroclinic eddy production rate which would go into the forward cascade in the model by von Storch et al. (2012) (Figure 3.8). The global transfer by this process amounts to  $0.31 \pm 0.23$  TW, i.e. only a fraction of the total production but comparable to the generation by lee waves. The flux by the forward cascade is not only large in the surface mixed layer where the stratification vanishes, or near the equator where geostrophic balance becomes a weaker constraint, but also at high latitudes in western boundary currents and the Southern Ocean, where the vertical shear becomes large.

We will assume that this energy transfer by the forward energy cascade at large  $Ri$  in the interior of the ocean generates gravity waves, while the remainder of the total eddy energy production is assumed to be dissipated by bottom friction. We will thus provide the flux by the forward cascade as an interior source to IDEMIX. The flux in the surface mixed layer will be assumed to contribute to small-scale

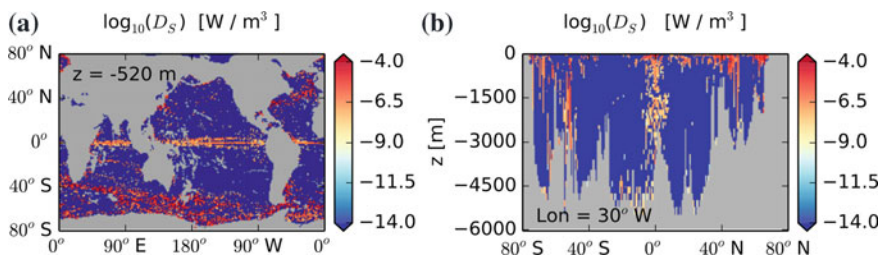


**Fig. 3.8** Horizontal and meridional sections of the implied energy transfer  $D_s$  due to the forward energy cascade in the high-resolution ocean model by von Storch et al. (2012). Taken from Brüggemann and Eden (2015)

turbulence there, while the flux near the equator within  $5^\circ$  latitude will be disregarded since here the inference from the simulations of mid-latitude baroclinic instability by Brüggemann and Eden (2015) might not hold. To include the interior flux in a version of IDEMIX coupled to a general circulation model, the dissipation of EKE implied by the mesoscale eddy closure by Eden and Greatbatch (2008b) will be used. Other proposed sources of eddy dissipation will be neglected in the first phase of this project, but will be considered in later phases if necessary.

Both, the bottom flux due to lee wave generation and the interior flux due to the forward energy cascade will be prescribed in a stand-alone version of the simple version of IDEMIX. Experiments with tidal and surface forcing with and without the flux due to the eddy dissipation will be compared with observational estimates of dissipation rates as in Figure 3.5 to identify and to validate the effect of eddy dissipation.

### 3.3.2 Including Wave–Mean Flow Interaction

Waves propagating in a vertically sheared mean flow exchange energy with the mean flow and can even break when they hit a critical layer or run into a wave capture domain. In the presence of a mean shear, the radiative transfer equation (3.9) for the energy spectrum correspondingly contains an exchange term with the mean flow (last term on the right-hand side). This exchange depends on the magnitude of the shear, internal wave energy, the direction of the wave propagation, and other wave properties. Assuming as before a fixed (but locally varying) form of the spectrum of unknown amplitude, it becomes possible to evaluate the effect of the wave–mean flow energy exchange for the energy compartments  $E^\pm$  integrated in wavenumber space, as shown in Olbers and Eden (2017), Eden and Olbers (2017). An extension of IDEMIX including the wave–mean flow energy exchange requires only the split of  $E^\pm$  or equivalently  $E$  and  $\Delta E$  into energy components which propagate in four different lateral directions, while all other parameters and closures remain identical to before. The corresponding IDEMIX model becomes

$$\begin{aligned}
 \partial_t E_e + \partial_z(c_0 \Delta E_e) &= -\tilde{U}_z \Delta E_e - \mu E_e (E_e + E_w) \\
 \partial_t \Delta E_e + \partial_z(c_0 E_e) &= -\tilde{U}_z E_e - \Delta E_e / \tau_v \\
 \partial_t E_w + \partial_z(c_0 \Delta E_w) &= \tilde{U}_z \Delta E_w - \mu E_w (E_e + E_w) \\
 \partial_t \Delta E_w + \partial_z(c_0 E_w) &= \tilde{U}_z E_w - \Delta E_w / \tau_v
 \end{aligned} \tag{3.25}$$

for eastward ( $E_e, \Delta E_e$ ) and westward propagating waves ( $E_w, \Delta E_w$ ), with  $\tilde{U}_z = (\sqrt{8}/\pi)\Lambda \partial_z U$ , and similar for northward ( $E_n, \Delta E_n$ ) and southward propagating waves ( $E_s, \Delta E_s$ ), except that  $\partial_z U$  is replaced with  $\partial_z V$ . The wave–mean flow interaction terms are those involving the mean shear. They derive from the last term in the radiation balance (3.9). The interaction coefficient  $\Lambda$  is computed in IDEMIX manner using the GM spectral shape (Olbers and Eden 2017).



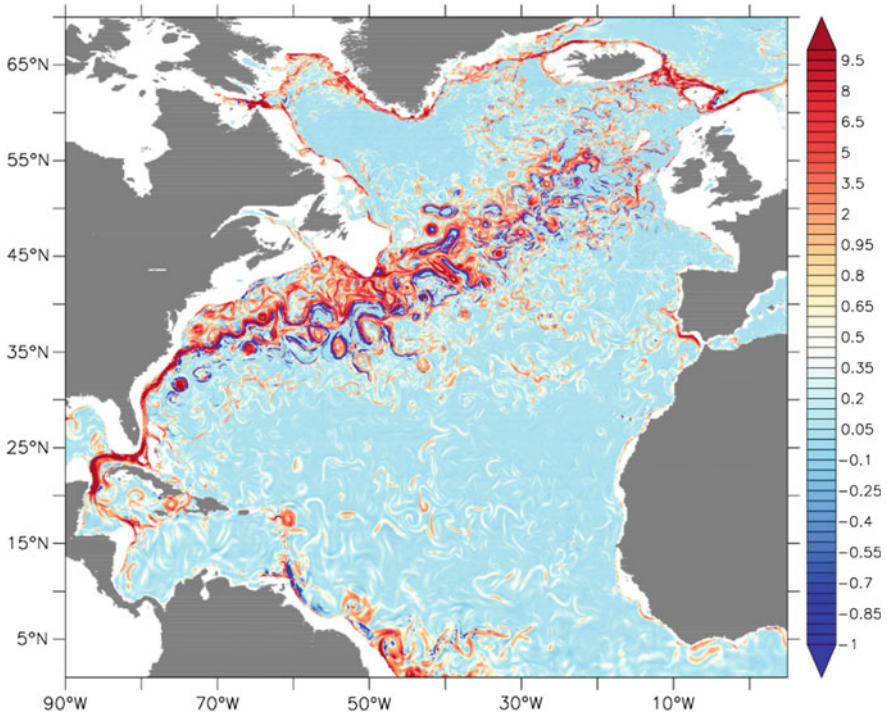


**Fig. 3.9** Instantaneous energy transfer from mean flow to waves in  $10^{-6}$  W/m<sup>3</sup> at 300 m depth in a high-resolution model of the North Atlantic Ocean. From Eden and Olbers (2017)

The effect on the mean flow figures then as a divergence of a vertical eddy momentum flux due to wave activity in the residual momentum equation, similar to vertical friction, although the direction of the energy exchange can be from the mean flow to the waves but also vice versa, as demonstrated in Figure 3.9. The figure shows the energy transfer from the mean flow to the waves due to wave drag at 300 m depth of a simulation with a realistic, eddying North Atlantic Ocean model for a snapshot in September. The energy transfer due to the wave drag is significant for the kinetic energy balance of the mean flow. At 300 m depth, the horizontally integrated energy transfer from the mean flow to the waves is  $19.9 \times 10^6$  W/m, while it is  $149.8 \times 10^6$  W/m for the dissipation due to lateral biharmonic friction. This ratio of 10 to 20% can also be found at other depths. The energy transfer from mean flow to small-scale turbulence by the parameterized vertical friction at 300 m depth amounts to  $56.9 \times 10^6$  W/m but is only significant within the mixed layer, and very low below; i.e. in the interior of the model, only lateral friction and the wave drag act as dissipation of mean kinetic energy. The depth-integrated values of the transfer due to lateral friction, wave drag, and vertical friction are  $0.224 \times 10^{12}$  W,  $0.018 \times 10^{12}$  W, and  $0.115 \times 10^{12}$  W, respectively. For the balance of internal wave energy itself,



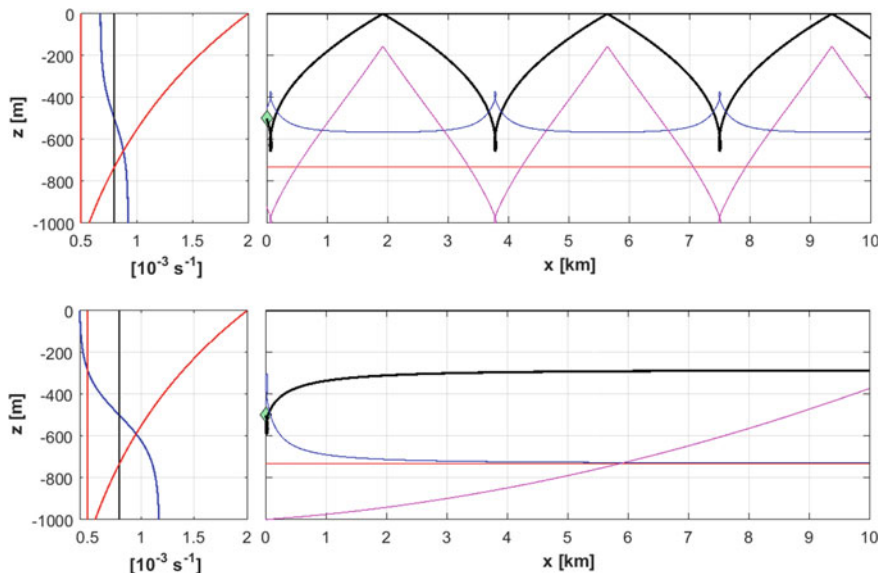


**Fig. 3.10** Rays for propagation in a vertical shear flow. Upper row: weak mean shear,  $U_0 = 0.1$ , lower row: strong mean shear,  $U_0 = 0.3$ . Left:  $f$  and  $N$  (red),  $\omega_{enc}$  (black),  $\omega(z) = \omega_{enc} - kU(z)$  (blue). Right: ray (black), energy  $E(t)$  (blue), minimum available energy  $fE(t_0)/\omega(t_0)$  (red), shear  $E(t)m^2(t)$  (magenta). Energy and shear have an unspecified scale. The horizontal wavelength is 5000 m. Other parameters are  $f = 5 \times 10^{-4} \text{ s}^{-1}$ ,  $N_0 = 2 \times 10^{-3} \text{ s}^{-1}$

the energy transfer due to the wave drag is less important, i.e. on the order of 5%, since the tidal forcing amounts to more than  $0.4 \times 10^{12} \text{ W}$  in the North Atlantic.

The effect of critical layers and wave capture, where waves break and contribute to density mixing, has not been discussed so far. The conditions for a generic case of a critical layer is  $N = \text{const}$  and a purely vertical shear flow  $\mathbf{U} = \mathbf{U}(z)$  so that the vertical wavenumber changes according to

$$\dot{m} = -\mathbf{k} \cdot \partial_z \mathbf{U} \quad (3.26)$$

such that  $|m|$  increases in time (linearly as  $\mathbf{k}$  remains constant) and the frequency  $\omega$  of the wave ultimately approaches  $f$  where the intrinsic group velocity goes to zero and the intrinsic propagation comes to a halt. At the same time the vertical wavelength diminishes, the wave is prone to break (in fact, as action is conserved,  $E(t)/\omega(t) = \text{const}$ , but the shear  $E(t)m^2(t)$  tends to infinity). We demonstrate the behaviour in an exponentially increasing Brunt-Väisälä frequency and a tanh-shaped mean flow in Figure 3.10 with different current amplitudes. The rays start at a depth of 500 m (at the zero of the mean current) and a downward group velocity. With a weak mean flow (upper panels), the shear does not yet allow a critical layer to appear. Note that the rays' cycle, energy, and shear are completely periodic. The situation changes dramatically (lower panels) when the shear is increased to an amplitude such that

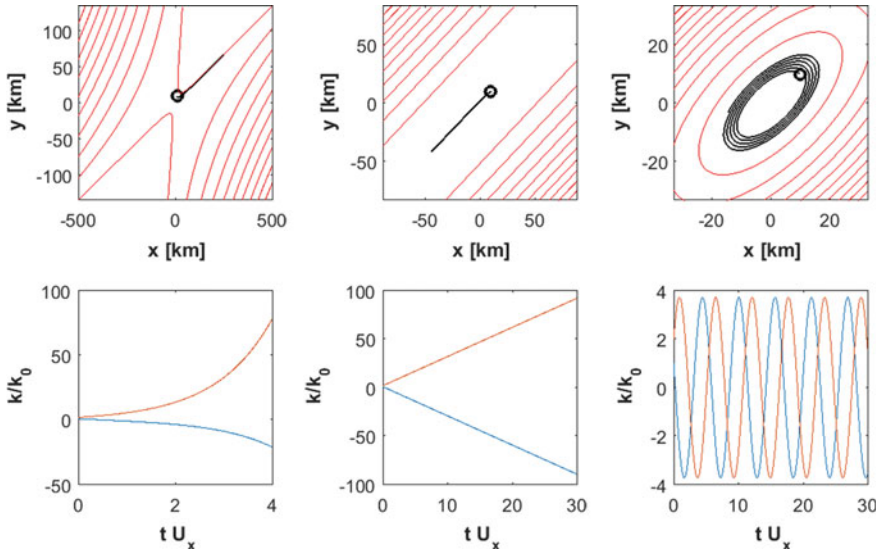


**Fig. 3.11** Generic cases of wave capture, after Bühler and McIntyre (2005). The streamfunction of the horizontal flow is  $\psi = -axy + c(x^2 + y^2)/2$  with  $U = -\psi_y = ax - cy$ ,  $V = \psi_x = -ay + cx$ . Hence,  $V_x + U_y = 0$ ,  $U_x + V_y = 0$ ,  $\beta = a^2 - c^2$ . Left:  $\beta > 0$ , hyperbolic case for  $c = a/2$ . Middle:  $\beta = 0$ , parabolic case. Right:  $\beta < 0$ , elliptic case for  $c = 3a/2$ . Upper panels: streamfunction (red) and ray (black). Lower panels:  $k_i/k_0$ ,  $i = 1, 2$  as function of time

at a certain level the intrinsic frequency can approach the local Coriolis frequency, i.e.  $\omega(z) = \omega_{enc} - \mathbf{k} \cdot \mathbf{U}(z) \rightarrow f$ . At such a level, the vertical group velocity goes to zero while the energy approaches the minimum value, however residing in ever decreasing vertical scales. The wave must eventually break.

A similar behaviour occurs in a flow with horizontal and vertical shear,  $\mathbf{U} = \mathbf{U}(\mathbf{x}, z)$  where the horizontal wave vector increases exponentially

$$\dot{\mathbf{k}} = -\mathbf{k} \cdot \partial_x \mathbf{U} \tag{3.27}$$

under certain conditions on the mean flow gradient. Equation (3.26) still holds such that  $|m|$  also increases exponentially. This is the generic case of wave capture. If  $U_z \sim U/H$ ,  $U_x \sim U/L$ , then the aspect ratio of the wavenumbers approaches  $m/k \sim L/H$  and the ratio of wavelength (vertical to horizontal) approaches  $H/L$ . The frequency of the wave in this state goes to  $\omega^2(t) \rightarrow f^2 + N^2(H/L)^2$  which is close to  $f^2$  (Bühler and McIntyre 2005). The group velocity is exponentially decreasing, and the wave will be captured (trapped) in the mean flow and break. Note, however, that the captured wave is still moving with the mean current. In Figure 3.11, we show wave capture for three generic cases of mean flow: a hyperbolic flow with a saddle point (the wavenumber increases exponentially), a parabolic case of parallel currents (the wavenumber increases linearly), and an elliptic case with closed streamlines (the

wavenumber shows a cyclic behaviour). In the first two cases, the wave is prone to breaking.

The critical layer process will be implemented by calculating the fraction of the vertical (up or down) flux of wave energy at any level that will eventually be absorbed in critical layers (at shallower or deeper levels) and contribute to mixing there. As for the other closures in IDEMIX, the assumption of a fixed spectral shape for the local wave energy will be used. The flux portion which is absorbed depends on the mean flow profile, on  $f/N$  and the total wave energy at the respective level. We will convert this flux portion directly into dissipation over the respective water column, obtaining a parameterization of the mixing induced by critical layer absorption. We attempt a similar treatment for wave capture.

### 3.3.3 Including Anisotropic Tidal Forcing

The linear theory by Bell (1975) can also be used to generate maps of energy transfers from the barotropic tide to internal waves, similar to the lee wave generation of a mean flow in (3.23). Two effects can lead to anisotropy in the wave generation: anisotropy in the barotropic flow (tidal ellipse) and anisotropy in the topography. A realistic estimate of the barotropic tidal velocity field is provided by the TPXO.7 model for eight tidal constituents ( $M_2$ ,  $S_2$ , etc.) with a resolution of  $1/4^\circ$  (Egbert et al. 2010). Anisotropic abyssal hill spectra are provided by the digital maps given by Goff and Arbic (2010), similar as used for (3.23), but to be implemented here in its anisotropic form on a 2 min horizontal grid. However, it is clear that also topographic variations with scales larger than about 10 km, not covered by the data set by Goff and Arbic (2010), will contribute to anisotropic baroclinic tide generation. Following Nycander (2005), we will also use the latest satellite-derived topography by Smith and Sandwell (1997) on a 2 min grid to extend the spectra by Goff and Arbic (2010) to smaller wavenumbers taken from the observed topography. Local two-dimensional spectral estimates of subregions of  $X$  km  $\times$   $X$  km size from the satellite-derived topography will be averaged and blended with the anisotropic spectrum by Goff and Arbic (2010), averaged over the same region.  $X$  and  $Y$  will be of order 50 to 100 km but varied to obtain the sensitivity on these parameters.

Based on this estimate of the topography spectrum and using the tidal velocity averaged over the same region for each tidal constituent, linear theory predicts the energy transfer to the baroclinic tides. We will use the spectral tapering method by Nycander (2005) to account for finite depth effects in the linear theory by Bell (1975). The flux  $\Phi_{tide}$  into the barotropic tide of frequency  $\omega_n$  and velocity amplitude  $|\mathbf{U}|$  for an isotropic tidal ellipse can be written as

$$\Phi_{tide}(\mathbf{k}) = \frac{1}{2} \rho_0 \frac{|\mathbf{U}|^2 N}{\omega_n \pi k_n k_s} \frac{h_{rms}^2 (\mu/2 - 1) (\omega_n^2 - f^2)^{1/2} k}{(1 + k^2/k_s^2 \cos^2(\theta - \theta_s) + k^2/k_n^2 \sin^2(\theta - \theta_s))^{\mu/2}} \quad (3.28)$$

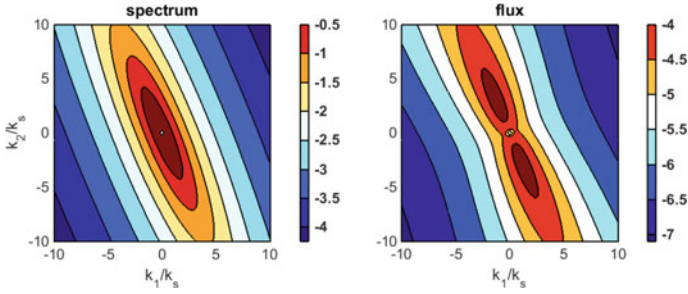


**Fig. 3.12** Example of an anisotropic tidal forcing (left) due to anisotropic topographic spectrum (right) given by the form of Goff and Arbic (2010). Both are shown as normalized functions of  $\mathbf{k} = (k_1, k_2)$  on a logarithm scale

as density in wavenumber space, where  $h_{rms}$  and  $\mu$  are defined above in Section 3.3.1.1 and where  $k_n$ ,  $k_s$ , and  $\theta_s$  define the anisotropy of the spectrum by Goff and Arbic (2010). The case with an anisotropic tidal ellipse is analogous but more involved. The resulting flux  $\Phi_{tide}$  is shown in Figure 3.12 as function of wavenumber vector  $\mathbf{k}$  for an artificial but typical topography spectrum based on the parameters given by Goff and Arbic (2010). The  $\phi$ -dependency of the forcing will generate a baroclinic tide propagating predominantly in the direction anticipated from the figure, which is clearly different from the isotropic flux used before by Eden and Olbers (2014), and we expect a corresponding effect of the improved forcing function for IDEMIX.

We will use  $\Phi_{tide}$  as interior forcing in (3.11) for the corresponding energy compartment in the extended version of IDEMIX. Expressing the  $\mathbf{k}$ -dependency of  $\Phi_{tide}$  in terms of vertical wavenumber  $m$  or vertical mode number, using the dispersion relation, it becomes also possible to determine from (3.28) the amount of energy transferred to the low modes and the amount transferred to the wave continuum. This will be an improvement of Eden and Olbers (2014) who simply transfer 50% to the continuum and 50% to the low modes. The flux  $\Phi_{tide}$  from (3.28) will be included in a stand-alone extended version of IDEMIX, and the results will be compared with observations.

### 3.3.4 Including High-Frequency Compartments

Waves forced at the base of the mixed layer by resonant surface–internal wave interaction (Olbers and Herterich 1979; Olbers and Eden 2016), mixed-layer turbulence (Bell 1978), and convective pumping (Polton et al. 2008) are of high frequency and thus trapped close to the surface. Their energy will thus predominantly contribute to near-surface mixing. Similar to the low-mode tidal and near-inertial energy compartments of the extended IDEMIX version by Eden and Olbers (2014), we

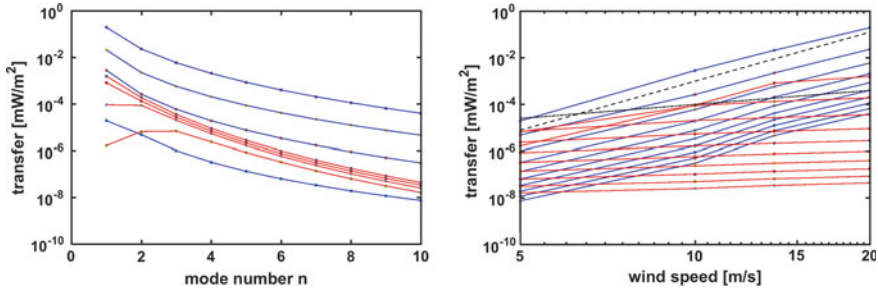


**Fig. 3.13** Transfer for SC (blue) and MI (red) mechanisms as function of mode number (left) and wind speed (right). The respective lowest curves are for wind speed 5 m/s or mode 10, and the uppermost is for wind speed 20 m/s and mode 1. The curves are for  $N_0 = 0.0157\text{s}^{-1}$ . The black dashed lines (right panel) display a  $U^2$  and  $U^7$  dependence. From Olbers and Eden (2016)

will split energy compartments of high-frequency and high vertical modes from the wave continuum and will treat them separately from the spectral continuum. This energy compartment couples to the wave continuum by induced diffusion, a process of wave–wave interactions (McComas 1977), across the boundaries in frequency domain and to the low vertical mode near-inertial waves. The waves described by this compartment are thought to break predominantly in the upper ocean and are thus of central importance for dissipation in and above the main thermocline.

Resonant triad interactions between surface gravity waves (SW, with frequencies  $\omega_j = \sqrt{gk_j}$ ,  $j = 1, 2$ ) and internal gravity waves (IW, with frequency  $\omega$ ) are hampered by the extreme difference of their frequencies in the resonance condition  $\omega_1 - \omega_2 - \omega = 0$ . The scattering cross section is of order  $(\omega^2/gk_j)^2 \ll 1$ . Two processes compete: spontaneous creation (SC) in which two SW generate an IW and modulation interaction (MI) where a preexisting internal wave is modulated by a surface wave and interacts with another one (Watson 1990; Olbers and Eden 2016). SC is always a source of IW energy, and MI might establish a damping of the internal wave field, thus acting against SC. Interesting is the dependence of the respective transfer rates on the wind speed  $U$  (via the spectral energy content of the SW spectrum). For MI, the rate varies as  $U^2$ , for SC however as  $U^7$ , so that the dominant process at low wind speeds (roughly  $U < 10$  m/s) is MI, while at stronger winds the interactions between surface and internal gravity waves are always controlled by SC (see Figure 3.13).

Figure 3.7 shows the annual mean total SC flux  $\Phi_{tot}$  and its maximum during the year entering the internal wave field diagnosed from a simulation with an ocean model which contains a mixed-layer parameterization after Gaspar et al. (1990). It is driven by wind stress forcing; this and also  $U$  are taken from the year 2010 of the reanalysis by Kalnay et al. (1996). The total SC flux is computed from a parameterization of the SC scattering integral, as explained in Olbers and Eden (2016), depending on the simulated mixed-layer depth, the Brunt-Väisälä frequency at the mixed-layer base, and the wind speed  $U$ . The largest fluxes show up in the storm track regions of the oceans, while towards the equator the flux and its maximum almost vanish.

The flux varies a lot in space and time. In the global integral, it is only about 0.5 to  $1 \times 10^{-3}$  TW, i.e. two orders of magnitude smaller than the flux due the inertial pumping. Locally in space and time, however, it can reach similar magnitudes. Since the internal waves generated by interaction with surface waves are of high frequency, their turning points lie close to the mixed layer. It is therefore likely that the flux  $\Phi_{tot}$  is also dissipated close to the mixed layer. This is different from the fluxes due to inertial pumping and the tides which generate low-frequency waves penetrating the entire depth range of the ocean. Our estimate of the implied dissipation shows that it sometimes reaches magnitudes comparable to observational estimates close to the mixed layer, in particular during strong wind events, but stays in general below them.

### 3.3.5 Evaluation with Available Observations

The results of the improved versions of IDEMIX need to be evaluated against observations. Measurements that resolve turbulence, however, are to date not available on a global scale. For the evaluation of IDEMIX, we therefore estimate dissipation rates of turbulent kinetic energy (TKE) and internal gravity wave energy from finestructure data, i.e. observations on 10–100 m vertical scales. The fundamental assumption of this ‘finestructure method’ is that TKE dissipation can be identified with the spectral energy transport caused by non-linear wave–wave interactions, which manifest themselves in the finescale variability of the internal wave field (Gregg 1989; Polzin et al. 1995). Based on the approach by Kunze et al. (2006) and Whalen et al. (2012), TKE-dissipation rates can be estimated from finescale strain information derived from Argo CTD profiles,<sup>6</sup>

$$\varepsilon = \varepsilon_0 \frac{\overline{N^2 \langle \xi_z^2 \rangle^2}}{N_0^2 \langle \xi_{z,GM}^2 \rangle^2} h(R_\omega) L(f, N), \quad (3.29)$$

where the observed strain variance  $\langle \xi_z^2 \rangle$  is scaled by the corresponding value for the GM model,  $\langle \xi_{z,GM}^2 \rangle$ ,  $L(f, N)$  is a function correcting for latitudinal variations, and  $\varepsilon_0$  is a constant. Due to the lack of shear information, the shear-to-strain ratio  $R_\omega$  has to be set constant, reducing the function  $h(R_\omega)$  to unity for the GM value of  $R_\omega = 3$ . Under the assumption that the observed internal gravity wave energy has the same wavenumber and frequency dependence as the GM model, it, too, can be estimated from finescale strain information (see Pollmann et al. 2017).

Figure 3.14 shows a comparison of Argo-derived and IDEMIX-based internal gravity wave energy levels. Like for dissipation rates (cf. Figure 3.5), IDEMIX well reproduces the magnitude as well as the spatial variations of the Argo-based estimates. Inconsistencies are, for example, found at high latitudes, e.g. in the northern

<sup>6</sup>The Argo programme maintains almost 4,000 freely drifting floats that profile temperature and salinity down to 2,000 m depth every 10 days, making the data publicly available within hours after their collection ([www.argo.ucsd.edu](http://www.argo.ucsd.edu)).

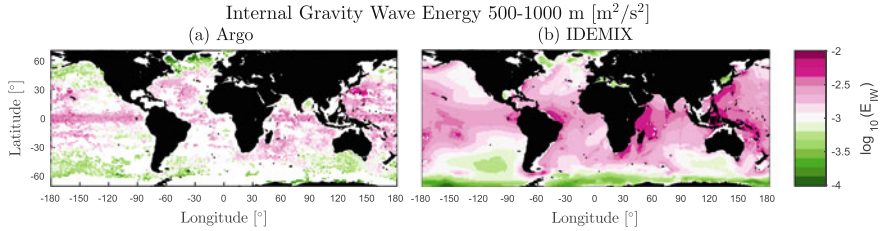


Fig. 3.14 Same as Figure 3.5 but for internal gravity wave energy. From Pollmann et al. (2017)

Pacific or Drake Passage, where IDEMIX simulates too high energy levels. In the 250–500 m depth range (not shown), this discrepancy is less pronounced, underlining the need to better understand and implement the depth dependence of the different forcing functions (e.g. the interaction with the mesoscale eddy field). Global estimates of internal gravity wave energies based on finescale strain information alone, like Figure 3.14, have to our knowledge not been attempted before.

The uncertainty of the Argo-derived dissipation rate and energy level estimates with respect to parameter choices and assumptions inherent in the finestructure method is shown in Figure 3.15. With variations amounting to more than a factor of two, the dissipation rate estimates prove more sensitive to modifications of the parameter settings than energy levels. Particularly, the value of the shear-to-strain

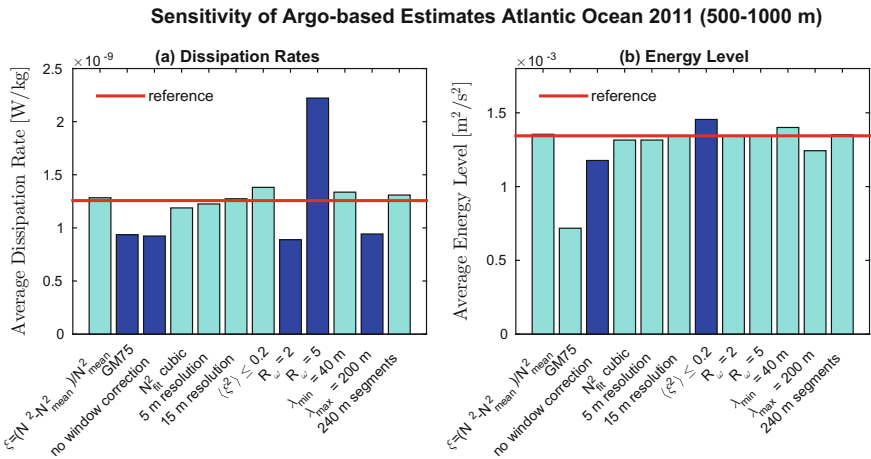


Fig. 3.15 Sensitivity of Argo-derived dissipation rate and energy level estimates: each bar represents a different scenario, where one parameter at a time was changed from the reference settings. These are given by  $\xi_z = (N^2 - N_{fit}^2)/N_{mean}^2$ , GM76 with  $A(m) \propto (m^2 + m_*^2)^{-1}$ , a resolution of 10 m,  $\langle \xi_z^2 \rangle \leq 0.1$ ,  $R_\omega = 3$ ,  $\lambda_{min} = 10$  m,  $\lambda_{max} = 100$  m and segments of 200 m length. Bars are shown in blue when the null hypothesis of a Welch's t-test, assuming equal mean dissipation rates in the reference case and the scenario in question, can be discarded for a significance level of  $\alpha = 0.05$ ; cyan bars denote the failure to do so. Modified after Pollmann et al. (2017)



ratio, which is observed to vary between 2 and 7 in the global ocean (Kunze et al. 2006), strongly affects the dissipation rates' magnitude. In total, technical and statistical uncertainties can accumulate to a factor of 6–8 uncertainty, but compensations between the different forms are possible. Since dissipation rates vary globally by three orders of magnitude, a general comparison to IDEMIX is still feasible in any case. We aim to reduce the bias of these comparisons, for example, by evaluating IDEMIX against improved dissipation rate estimates that are based on a combination of shear and strain information.

### 3.4 Atmospheric Processes in IDEMIX

Important processes which generate gravity waves in the atmosphere are large-scale flow over orography, convection as well as spontaneous emission from jet streams, fronts, and other balanced flows. The waves propagate vertically and laterally over large distances and interact with the mean flow, and they feed energy to small-scale turbulence when they break. While in the ocean the density-mixing effect during wave breaking is considered to be most important since it generates potential energy and thus drives large-scale flow, it is the wave–mean flow interaction known as momentum and energy deposition that is most important in the atmosphere (e.g. Miller et al. 1989). Regarding the atmosphere, the momentum deposition, also known as gravity wave drag, is in the focus of parameterization schemes since it strongly contributes to driving the residual circulation in the middle atmosphere, to constrain the tropospheric jets, and to induce the quasi-biennial oscillation in the tropical stratosphere. The turbulent frictional heating that accompanies wave breaking becomes important in the middle atmosphere and needs consistent treatment as part of the energy deposition (Becker 2004). In contrast, this heating can be safely neglected in the ocean (McDougall 2003; Olbers et al. 2012; Eden 2015).

In general circulation models of the atmosphere, the gravity wave field is only marginally resolved and its effects on the mean flow need to be parameterized. The first theory that gave rise to simple gravity wave parameterizations in global circulation models is the saturation concept by Lindzen (1981). Here, upward propagating monochromatic waves are assumed to be damped by turbulent vertical diffusion above a certain critical height such that convective instability is marginally avoided. This wave damping leads to non-conservative wave–mean flow interaction according to the non-acceleration theorem (Andrews and McIntyre 1976). Other damping mechanisms are possible as well. For example, gravity wave schemes may employ a spectrum of waves that is truncated with height due to some criterion at the high vertical wavenumber end (Hines 1997; Alexander and Dunkerton 1999; Warner and McIntyre 2001). Lindzen's simple wave saturation concept has also been applied to orographic gravity waves by McFarlane (1987), and corresponding schemes are currently used in many climate models in order to simulate realistic jets in the troposphere and winter stratosphere. The response of orographic gravity waves is particularly essential in climate scenarios with regard to changes in the Brewer–Dobson

circulation (McLandress and Shepherd 2009). A basic overview of the wave driving of the middle atmosphere is given by Becker (2012).

Non-orographic gravity waves are sometimes also parameterized by concepts which go beyond linear theory, such as, for example, the Doppler spread theory (Hines 1997), where not only the Doppler shift by the mean flow but also that by the entire spectrum of parameterized waves is considered as a criterion for spectral truncation. Another example is the non-linear saturation theory of Medvedev and Klaasen (e.g. Yiğit et al. 2008), where non-linear wave interactions are assumed to trigger convective instabilities leading to a wave-induced eddy diffusion, as a first step towards accounting for the effect of resonant wave–wave interaction. Overviews of the gravity wave schemes currently used in global models are given in Fritts and Alexander (2003) and Alexander et al. (2010).

We emphasize that all conventional gravity wave schemes are based on the framework of the single-column approximation, as well as on the strong assumptions of a stationary background state and a stationary wave energy equation (see discussion in Becker and McLandress 2009). Conservative (reversible) wave–mean flow interactions, which may take place when a wave packet propagates through a vertically variable background atmosphere, are excluded in such a framework. Furthermore, the wave parameters have to be specified at a particular launch level; sources that are continuous in space and time, e.g. due to convection or frontal activity, cannot be incorporated in a consistent fashion. The latter restriction holds even for more sophisticated parameterizations that are based on ray tracing (Dunkerton and Fritts 1984; Warner and McIntyre 1996; Preusse et al. 2009; Senf and Achatz 2011). Conventional gravity wave schemes often also lack a consistent representation of scale interactions and energetics (Becker 2004; Becker and McLandress 2009). Particularly, the stationarity assumptions lead to parameterization errors when the interaction between gravity waves and thermal tides (having planetary scales and periods of 8, 12, and 24 hours) is considered. As shown by Senf and Achatz (2011), gravity wave–tidal interaction changes significantly when a non-stationary parameterization based on the full ray tracing equations is used instead of the conventional framework. One particular reason is that the horizontal phase speed (or ground-based frequency) of a gravity wave changes when the background wind is temporally variable (Fritts and Dunkerton 1984). In addition, horizontal propagation and refraction play an important role for gravity wave propagating from the lower to the middle atmosphere (Preusse et al. 2009; Fritts et al. 2006), but is neglected in the single-column approximation.

Müller and Natarov (2003) suggested to base a model for internal waves in the ocean on the radiative transfer equation of weakly interacting gravity waves (Hasselmann 1968), a concept which has—to our knowledge—never been considered for gravity wave parameterizations for the atmosphere. This equation describes (1) the propagation and refraction of the gravity wave field in physical and wavenumber space, (2) the wave–mean flow interaction, (3) non-linear wave–wave interactions, and (4) the forcing and dissipation of the waves. Olbers and Eden (2013) considered a drastic simplification of the concept which they called IDEMIX (Internal wave Dissipation, Energy and Mixing). Instead of resolving the detailed wave spectrum

as proposed in Müller and Natarov (2003), they integrate the radiative transfer equation in the wavenumber and frequency domain, leading to conservation equations for integral energy compartments in physical space, which can be closed with a few simple but reasonable parameterizations. The IDEMIX concept yields an energetically consistent framework to describe wave effects and has been shown to be successful for ocean applications. We propose to follow this approach and to base a new, energetically consistent gravity wave parameterization for atmosphere models on the radiative transfer equation. Applying the IDEMIX concept will also foster transfer of knowledge from the oceanic community to the atmospheric community and vice versa.

Integrating the radiative transfer equation in wavenumber space yields prognostic equations in physical space for energy compartments describing the mean wave propagation, refraction, and wave–mean flow interaction, and the integrated effects of wave–wave interaction, forcing and dissipation. The key to describe the mean propagation, refraction, and wave–mean flow interaction of the compartments in IDEMIX is the assumption that the actual wave spectrum is close to a wave spectrum of known shape but unknown amplitude. In the ocean, this would be the well-known Garrett–Munk spectrum (e.g. Garrett and Munk 1972). In the atmosphere, it would be a different shape as described, for example, by Fritts and VanZandt (1993) or Nastrom and Gage (1985), which was also assumed in the scheme by Warner and McIntyre (2001). The free parameters of the energy compartments are then used as additional prognostic variables in a circulation model. Olbers and Eden (2013) use only two energy compartments for the up- and downward propagating part of the full spectrum in a simple IDEMIX version. The wave–wave interaction is parameterized as linear decay of the asymmetry in the vertical propagation, and the dissipation of wave energy is given by a quadratic functional of total wave energy (Olbers 1976; Gregg 1989; Müller et al. 1986). In the atmospheric case, we will have different compartments for different directions of horizontal phase propagation, and it is sufficient to consider only upward group propagation.

Recently, IDEMIX was extended by single-column approximation of wave–mean flow interaction (Olbers and Eden 2017; Eden and Olbers 2017). Figure 3.16 shows wave energy compartments in a one-dimensional  $(z, t)$  idealized simulation using IDEMIX with waves propagating through a mean flow with vertical shear that is concentrated in the upper part of the domain. The waves are forced from below with a magnitude representative of oceanic tidal forcing. Shown are energy compartments of east- and westward and up- and downward propagating waves. The governing equations are given by (3.25). While up- and eastward (Figure 3.16b) and down- and westward (Figure 3.16c) propagating waves lose energy to the mean flow, down- and eastward (Figure 3.16a) and up- and westward (Figure 3.16d) propagating waves gain energy from the mean flow, while they propagate through the shear zone. Note that changes in wave energy outside the shear zone are only due to the variable buoyancy frequency. Without dissipation, the energy exchange of the waves with the mean flow would be completely reversible. Up- and eastward propagating wave lose energy, but are reflected at the surface to down- and eastward propagating waves and regain the same amount of energy; then, they are reflected at the bottom, lose

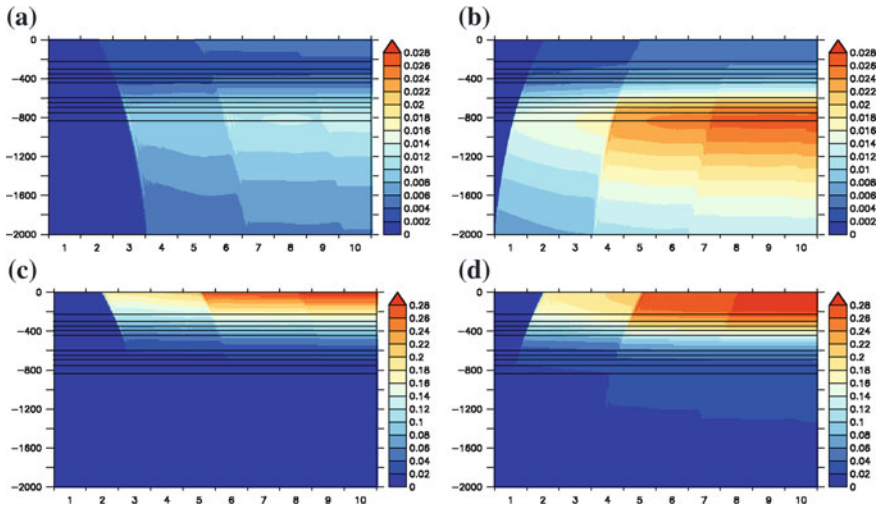


**Fig. 3.16** Energy compartments in an idealized IDEMIX simulation as a function of height  $z$  and time  $t$ . Solid lines denote the shear zone. (a) Energy compartment of down- and eastward propagating, (b) of up- and eastward propagating, (c) down- and westward propagating, and (d) up- and westward propagating waves. Note the different colour scales in the upper and lower row. Energy magnitudes are representative of oceanic waves forced by the barotropic tidal flow at the bottom. From Olbers and Eden (2017)

energy, and so forth. The same is true for the westward propagating waves. Only if there is dissipation, as in the simulation shown in Figure 3.16, this symmetry is broken and a net energy exchange with the mean flow takes place. Note that this behaviour of IDEMIX is fully consistent with the non-acceleration theorem of Andrews and McIntyre (1976). In the atmosphere, surface reflection is missing and reversible energy exchanges with the mean flow are less likely than in the ocean, such that irreversible wave–mean flow interaction is of significant importance for the large-scale circulation. For a mean shear as shown in Figure 3.16, the energy transfer is from the mean flow to the waves, which is akin to a wave drag, but other configurations (jet-like situations) can also lead to an acceleration of the mean flow by the waves.

### 3.5 Summary

The recently proposed parameterization module IDEMIX (Internal wave Dissipation Energy and Mixing) describes the generation, propagation, interaction, and dissipation of the internal gravity wave field and can be used in ocean general circulation models to account for vertical mixing (and friction) in the interior of the ocean. It is based on the radiative transfer equation of a weakly interacting internal wave field,

for which spectrally integrated energy compartments are used as prognostic model variables. IDEMIX is central to the concept of an energetically consistent ocean model, since it enables to link all sources and sinks of internal wave energy and furthermore all parameterized forms of energy in an ocean model without spurious sources and sinks of energy.

In its simplest version, IDEMIX consists of two energy compartments of interacting up- and downward propagating waves; in a more detailed version, low vertical mode compartments at near-inertial and frequencies of tidal constituents are added which also account for horizontally anisotropic wave propagation. It is proposed to extend IDEMIX

- with forcing mechanism by mesoscale eddy dissipation, such as lee wave generation or spontaneous wave emission of balanced flow
- with the effect of the interaction of the internal wave field with mesoscale and large-scale mean flow including critical layers and wave capture
- with anisotropic forcing of the low-mode tidal energy compartments
- and with additional energy compartments for high-frequency, high-wavenumber waves which are in particular effective for upper ocean mixing.

All these processes have never been implemented in ocean models but have an important effect on mixing and the energy transfers in the ocean. We will validate the simple and more complex versions of IDEMIX and the new version using available fine- and microstructure data sets. The simple and more complex IDEMIX versions will be implemented into the ICON and FESOM ocean models. By linking the wave sources with the wave dissipation using IDEMIX both in the ocean and atmosphere, we envision to close the energy cycle in a consistent way for the coupled system.

Gravity waves are an important part of the energy cycle of the atmosphere and exchange momentum and energy with the mean flow due to wave breaking and wave refraction. Wave breaking and the resulting mean flow effects need special parameterization in global climate models as they usually resolve at most a small part of the full spectrum of gravity waves. Here, we apply the IDEMIX concept to develop corresponding gravity wave schemes for atmospheric circulation models. We propose to base a new, energetically consistent gravity wave parameterization on the radiative transfer equation for a field of waves. This method is fundamentally different from conventional schemes which describe the superposition of monochromatic waves launched at a particular level and which make the strong assumption of a stationary mean flow.

The IDEMIX concept was shown to be successful for ocean applications, but instead of focussing on the mixing effect by breaking waves as for the oceanic case, the focus in the atmospheric application is on the wave–mean flow interaction, i.e. the gravity wave drag and the energy deposition. We will extend the concept of energetically consistent closures to atmospheric gravity wave closures. We will derive gravity wave source functions due to flow over orography and due to the forcing by frontal dynamics and convection. We will include the effects of transience of the mean flow on the gravity wave field, and we will allow to incorporate sinks and sources that are continuous in space and time. During the first phase of the project, we will

stick to the single-column approximation in order to allow for easy implementation of the derived gravity wave scheme in global circulation models.

There are several ways to generalize the proposed gravity wave scheme. The most obvious one is to use the general dispersion relation for gravity waves such as to incorporate also high-frequency and inertial-gravity waves. In the latter case, the momentum flux must be substituted by the pseudo-momentum flux in order to account for the Stokes drift when  $\omega$  approaches the Coriolis parameter (Fritts and Alexander 2003), as is in principle always the case close to a critical level. Furthermore, we may dispense with discrete azimuths and rather use a continuous directional representation, thereby modifying also the radiative transfer equation (3.13). Furthermore, one should consider existing theories to account for non-linear effects and wave-wave interaction in the wave-breaking process (Yiğit et al. 2008) and incorporate this insight into the new framework. Simple closures for the wave-wave interaction in the oceanic case are outlined in Olbers and Eden (2013) and may be considered also for atmospheric case. Finally, we may relax the single-column approach and consider wave propagation and refraction in all three directions.

## References

- Alexander, M., Dunkerton, T.: A spectral parameterization of mean-flow forcing due to breaking gravity waves. *J. Atmos. Sci.* **56**(24), 4167–4182 (1999)
- Alexander, M., Geller, M., McLandress, C., Polavarapu, S., Preusse, P., Sassi, F., Sato, K., Eckermann, S., Ern, M., Hertzog, A., et al.: Recent developments in gravity-wave effects in climate models and the global distribution of gravity-wave momentum flux from observations and models. *Q. J. R. Meteorol. Soc.* **136**(650), 1103–1124 (2010)
- Alford, M.: Internal swell generation: the spatial distribution of energy flux from the wind to mixed layer near-inertial motions. *J. Phys. Oceanogr.* **31**(8), 2359–2368 (2001)
- Andrews, D.G., McIntyre, M.E.: Planetary waves in horizontal and vertical shear: the generalized Eliassen-Palm relation and the zonal mean acceleration. *J. Atmos. Sci.* **33**, 2031–2048 (1976)
- Arbic, B.K., Shriver, J.F., Hogan, P.J., Hurlburt, H.E., McClean, J.L., Metzger, E.J., Scott, R.B., Sen, A., Smedstad, O.M., Wallcraft, A.J.: Estimates of bottom flows and bottom boundary layer dissipation of the oceanic general circulation from global high-resolution models. *J. Geophys. Res.* **114**(C2) (2009)
- Becker, E.: Direct heating rates associated with gravity wave saturation. *J. Atmos. Sol. Terr. Phys.* **66**(6), 683–696 (2004)
- Becker, E.: Dynamical control of the middle atmosphere. *Space Sci. Rev.* **168**(1–4), 283–314 (2012)
- Becker, E., McLandress, C.: Consistent scale interaction of gravity waves in the Doppler spread parameterization. *J. Atmos. Sci.* **66**(5), 1434–1449 (2009)
- Bell, T.H.: Topographically generated internal waves in the open ocean. *J. Geophys. Res.* **80**(3), 320–327 (1975)
- Bell, T.H.: Radiation damping of inertial oscillations in the upper ocean. *J. Fluid Mech.* **88**(02), 289–308 (1978)
- Bender, C.M., Orszag, S.A.: *Advanced Mathematical Methods for Scientists and Engineers: Asymptotic Methods and Perturbation Theory*. McGraw-Hill Book Company, New York (1978)
- Berry, M.V., Mount, K.: Semiclassical approximations in wave mechanics. *Rep. Prog. Phys.* **35**(1), 315–397 (1972)

- Bretherton, F.P., Garrett, C.J.: Wavetrains in inhomogeneous moving media. In: Proceedings of the Royal Society of London A: Mathematical, Physical and Engineering Sciences, vol. 302, pp. 529–554. The Royal Society (1968)
- Brüggemann, N., Eden, C.: Routes to dissipation under different dynamical conditions. *J. Phys. Oceanogr.* **45**(8), 2149–2168 (2015)
- Bryan, K., Lewis, L.: A water mass model of circulation cells and the source waters of the Pacific equatorial undercurrent. *J. Phys. Oceanogr.* **28**, 62–84 (1979)
- Bühler, O., McIntyre, M.E.: Wave capture and wave-vortex duality. *J. Fluid Mech.* **534**, 67–95 (2005)
- Cairns, J.L., Williams, G.O.: Internal wave observations from a midwater float, 2. *J. Geophys. Res.* **81**(12), 1943–1950 (1976)
- Charron, M., Manzini, E.: Gravity waves from fronts: Parameterization and middle atmosphere response in a general circulation model. *J. Atmos. Sci.* **59**(5), 923–941 (2002)
- Cummins, P.F., Holloway, G., Gargett, A.E.: Sensitivity of the GFDL ocean general circulation model to a parameterization of vertical diffusion. *J. Phys. Oceanogr.* **20**, 817–830 (1990)
- Desaubies, Y.J.: Analytical representation of internal wave spectra. *J. Geophys. Res.* **6**(6), 976–981 (1976)
- Dewar, W.K., Hogg, A.M.: Topographic inviscid dissipation of balanced flow. *Ocean Model.* **32**(1), 1–13 (2010)
- Dunkerton, T.J., Fritts, D.C.: Transient gravity wave-critical layer interaction. Part I: convective adjustment and the mean zonal acceleration. *J. Atmos. Sci.* **41**(6), 992–1007 (1984)
- Dushaw, B.D., Worcester, P.F., Dzieciuch, M.A.: On the predictability of mode-1 internal tides. *Deep-Sea Res.* **58**(6), 677–698 (2011)
- Eden, C.: Revisiting the energetics of the ocean in Boussinesq approximation. *J. Phys. Oceanogr.* **45**(3), 630–637 (2015)
- Eden, C., Czeschel, L., Olbers, D.: Towards energetically consistent ocean models. *J. Phys. Oceanogr.* **44**(8), 2093–2106 (2014)
- Eden, C., Greatbatch, R.J.: Diapycnal mixing by mesoscale eddies. *Ocean Model.* **23**, 113–120 (2008a)
- Eden, C., Greatbatch, R.J.: Towards a mesoscale eddy closure. *Ocean Model.* **20**, 223–239 (2008b)
- Eden, C., Olbers, D.: An energy compartment model for propagation, non-linear interaction and dissipation of internal gravity waves. *J. Phys. Oceanogr.* **44**, 2093–2106 (2014)
- Eden, C., Olbers, D.: Interaction of internal waves with a mean flow. Part II: wave drag. *J. Phys. Oceanogr.* **47**, 1403–1412 (2017)
- Egbert, G.D., Erofeeva, S.Y., Ray, R.D.: Assimilation of altimetry data for nonlinear shallow-water tides: quarter-diurnal tides of the Northwest European Shelf. *Cont. Shelf Res.* **30**(6), 668–679 (2010)
- Ford, R., McIntyre, M., Norton, W.: Balance and the slow quasimanifold: some explicit results. *J. Atmos. Sci.* **57**(9), 1236–1254 (2000)
- Fritts, D.C., Alexander, M.J.: Gravity wave dynamics and effects in the middle atmosphere. *Rev. Geophys.* **41**(1) (2003)
- Fritts, D.C., Dunkerton, T.J.: A quasi-linear study of gravity-wave saturation and self-acceleration. *J. Atmos. Sci.* **41**(22), 3272–3289 (1984)
- Fritts, D.C., Vadas, S.L., Wan, K., Werne, J.A.: Mean and variable forcing of the middle atmosphere by gravity waves. *J. Atmos. Sol. Terr. Phys.* **68**(3), 247–265 (2006)
- Fritts, D.C., VanZandt, T.E.: Spectral estimates of gravity wave energy and momentum fluxes. Part I: energy dissipation, acceleration, and constraints. *J. Atmos. Sci.* **50**(22), 3685–3694 (1993)
- Garcia, R., Marsh, D., Kinnison, D., Boville, B., Sassi, F.: Simulation of secular trends in the middle atmosphere, 1950–2003. *J. Geophys. Res.* **112**(D9) (2007)
- Garrett, C.: What is the near-inertial wave band and why is it different from the rest of the internal wave spectrum? *J. Phys. Oceanogr.* **31**, 962–71 (2001)
- Garrett, C., Munk, W.: Space-time scales of internal waves. *Geophys. Astrophys. Fluid Dyn.* **3**(1), 225–264 (1972)



- Garrett, C., Munk, W.: Space-time scales of internal waves: a progress report. *J. Geophys. Res.* **80**, 291–297 (1975)
- Gaspar, P., Gregoris, Y., Lefevre, J.-M.: A simple eddy kinetic energy model for simulations of the oceanic vertical mixing: tests at station PAPA and Long-Term Upper Ocean Study site. *J. Geophys. Res.* **95**, 16179–16193 (1990)
- Goff, J.A., Arbic, B.K.: Global prediction of abyssal hill roughness statistics for use in ocean models from digital maps of paleo-spreading rate, paleo-ridge orientation, and sediment thickness. *Ocean Model.* **32**(1), 36–43 (2010)
- Gregg, M.C.: Scaling turbulent dissipation in the thermocline. *J. Geophys. Res.* **94**(C7), 9686–9698 (1989)
- Hasselmann, K.: Weak-interaction theory of ocean waves. *Basic Dev. Fluid Dyn.* **2**, 117–182 (1968)
- Hasselmann, K., Barnett, T., Bouws, E., Carlson, H., Cartwright, D., Enke, K., Ewing, J., Gienapp, H., Hasselmann, D., Krusemann, P., Meerburg, A., Müller, P., Olbers, D., Richter, K., Sell, W., Walden, H.: Measurements of wind-wave growth and swell decay during the Joint North Sea Wave Project (JONSWAP). *Dtsch. Hydrogr. Z.* **12**, 1–95 (1973)
- Hines, C.O.: Doppler-spread parameterization of gravity-wave momentum deposition in the middle atmosphere. Part 1: basic formulation. *J. Atmos. Sol. Terr. Phys.* **59**(4), 371–386 (1997)
- Jayne, S., St. Laurent, L.: Parameterizing tidal dissipation over rough topography. *Geophys. Res. Lett.* **28**(5), 811–814 (2001)
- Jones, W.L.: Ray tracing for internal gravity waves. *J. Geophys. Res.* **74**(8), 2028–2033 (1969)
- Kalnay, E., Kanamitsu, M., Kistler, R., Collins, W., Deaven, D., Gandin, L., Iredell, M., Saha, S., White, G., Woollen, J., Zhu, Y., Chelliah, M., Ebisuzaki, W., Higgins, W., Janowiak, J., Mo, K., Ropelewski, C., Wang, J., Leetmaa, A., Reynolds, R., Jenne, R., Joseph, D.: The NCEP/NCAR 40-years reanalysis project. *Bull. Am. Meteorol. Soc.* **77**, 437–471 (1996)
- Kunze, E., Firing, E., Hummon, J.M., Chereskin, T.K., Thurnherr, A.M.: Global abyssal mixing inferred from lowered ADCP shear and CTD strain profiles. *J. Phys. Oceanogr.* **36**(8), 1553–1576 (2006)
- Kunze, E., Smith, S.L.: The role of small-scale topography in turbulent mixing of the global ocean. *Oceanography* **17**(1), 55–64 (2004)
- Landau, L.D., Lifshitz, E.M.: *Mechanics, Course of Theoretical Physics*, vol. 1. Pergamon Press Ltd. (1982)
- Lighthill, M.J.: On sound generated aerodynamically. I. General theory. In: *Proceedings of the Royal Society of London A: Mathematical, Physical and Engineering Sciences*, vol. 211, pp. 564–587. The Royal Society (1952)
- Lindzen, R.S.: Turbulence and stress owing to gravity wave and tidal breakdown. *J. Geophys. Res.* **86**(C10), 9707–9714 (1981)
- McComas, C., Müller, P.: Time scales of resonant interactions among oceanic internal waves. *J. Phys. Oceanogr.* **11**, 139–147 (1981)
- McComas, C.H.: Equilibrium mechanisms within the oceanic internal wave field. *J. Phys. Oceanogr.* **7**, 836–845 (1977)
- McDougall, T.J.: Potential enthalpy: a conservative oceanic variable for evaluating heat content and heat fluxes. *J. Phys. Oceanogr.* **33**(5), 945–963 (2003)
- McFarlane, N.: The effect of orographically excited gravity wave drag on the general circulation of the lower stratosphere and troposphere. *J. Atmos. Sci.* **44**(14), 1775–1800 (1987)
- McLandress, C., Shepherd, T.G.: Simulated anthropogenic changes in the brewer-dobson circulation, including its extension to high latitudes. *J. Clim.* **22**(6), 1516–1540 (2009)
- Miller, M., Palmer, T., Swinbank, R.: Parametrization and influence of subgridscale orography in general circulation and numerical weather prediction models. *Meteorol. Atmos. Phys.* **40**(1–3), 84–109 (1989)
- Molemaker, M.J., McWilliams, J.C., Yavneh, I.: Baroclinic instability and loss of balance. *J. Phys. Oceanogr.* **35**, 1505 (2005)
- Molemaker, M.J., McWilliams, J. C., Capet, X.: Balanced and unbalanced routes to dissipation in an equilibrated Eady flow. *J. Fluid Mech.* **654**, 35–63 (2010)

- Müller, M., Cherniawsky, J., Foreman, M., Storch, J.-S.: Global M2 internal tide and its seasonal variability from high resolution ocean circulation and tide modeling. *Geophys. Res. Lett.* **39**(19) (2012)
- Müller, P.: On the diffusion of momentum and mass by internal gravity waves. *J. Fluid Mech.* **77**(04), 789–823 (1976)
- Müller, P., Holloway, G., Henyey, F., Pomphrey, N.: Nonlinear interactions among internal gravity waves. *Rev. Geophys.* **24**(3), 493–536 (1986)
- Müller, P., Natarov, A.: The internal wave action model (IWAM). In: Proceedings, 13th Aha Huliko‘a Hawaiian Winter Workshop, School of Ocean and Earth Science and Technology, Special Publication (2003)
- Müller, P., Olbers, D.J.: On the dynamics of internal waves in the deep ocean. *J. Geophys. Res.* **80**, 3848–3860 (1975)
- Müller, P., Olbers, D.J., Willebrand, J.: The IWEX spectrum. *J. Geophys. Res.* **83**, 479–500 (1978)
- Munk, W.: Internal waves and small-scale processes. In: Warren, B.A., Wunsch, C. (eds.) *Evolution of Physical Oceanography*, pp. 264–291. MIT Press, Cambridge, MA (1981)
- Nastrom, G., Gage, K.S.: A climatology of atmospheric wavenumber spectra of wind and temperature observed by commercial aircraft. *J. Atmos. Sci.* **42**(9), 950–960 (1985)
- Nikurashin, M., Ferrari, R.: Global energy conversion rate from geostrophic flows into internal lee waves in the deep ocean. *Geophys. Res. Lett.* **38**, L08610 (2011)
- Nycander, J.: Generation of internal waves in the deep ocean by tides. *J. Geophys. Res.* **110**(C9), C10028 (2005)
- Olbers, D., Eden, C.: A global model for the diapycnal diffusivity induced by internal gravity waves. *J. Phys. Oceanogr.* **43**, 1759–1779 (2013)
- Olbers, D., Eden, C.: Revisiting the generation of internal waves by resonant interaction with surface waves. *J. Phys. Oceanogr.* **46**, 2335–2350 (2016)
- Olbers, D., Eden, C.: Interaction of internal waves with a mean flow. Part I: energy conversion. *J. Phys. Oceanogr.* **47**, 1389–1401 (2017)
- Olbers, D., Willebrand, J., Eden, C.: *Ocean Dynamics*. Springer, Heidelberg (2012)
- Olbers, D.J.: Nonlinear energy transfer and the energy balance of the internal wave field in the deep ocean. *J. Fluid Mech.* **74**, 375–399 (1976)
- Olbers, D.J.: Models of the oceanic internal wave field. *Rev. Geophys. Space Phys.* **21**, 1567–1606 (1983)
- Olbers, D.J.: Internal gravity waves. In: Stündermann, J. (ed.) *Landolt-Börnstein—Numerical Data and Functional Relationships in Science and Technology—New Series, Group V, vol. 3a*, pp. 37–82. Springer, Berlin (1986)
- Olbers, D.J., Herterich, K.: The spectral energy transfer from surface waves to internal waves. *J. Fluid Mech.* **92**, 349–379 (1979)
- Osborn, T.R., Cox, C.S.: Oceanic fine structure. *Geophys. Astrophys. Fluid Dyn.* **3**, 321–345 (1972)
- Pollmann, F., Eden, C., Olbers, D.: Evaluating the global internal wave model IDEMIX using a finescale strain approximation. *J. Phys. Oceanogr.* **47**, 2267–2289 (2017)
- Polton, J.A., Smith, J.A., MacKinnon, J.A., Tejada-Martínez, A.E.: Rapid generation of high-frequency internal waves beneath a wind and wave forced oceanic surface mixed layer. *Geophys. Res. Lett.* **35**(13) (2008)
- Polzin, K.L.: Mesoscale eddy-internal wave coupling. Part I: symmetry, wave capture, and results from the mid-ocean dynamics experiment. *J. Phys. Oceanogr.* **38**(11), 2556–2574 (2008)
- Polzin, K.L., Lvov, Y.V.: Toward regional characterizations of the oceanic internal wavefield. *Rev. Geophys.* **49**(4), RG4003 (2011)
- Polzin, K.L., Toole, J.M., Schmitt, R.W.: Finescale parameterizations of turbulent dissipation. *J. Phys. Oceanogr.* **25**(3), 306–328 (1995)
- Preusse, P., Eckermann, S.D., Ern, M., Oberheide, J., Picard, R.H., Roble, R.G., Riese, M., Russell, J.M., Mlynczak, M.G.: Global ray tracing simulations of the saber gravity wave climatology. *J. Geophys. Res.* **114**(D8) (2009)

- Richter, J.H., Sassi, F., Garcia, R.R.: Toward a physically based gravity wave source parameterization in a general circulation model. *J. Atmos. Sci.* **67**(1), 136–156 (2010)
- Rimac, A., von Storch, J.-S., Eden, C., Haak, H.: The influence of high-resolution wind stress field on the power input to near-inertial motions in the ocean. *Geophys. Res. Lett.* **40**(18), 4882–4886 (2013)
- Scinocca, J.F.: An accurate spectral nonorographic gravity wave drag parameterization for general circulation models. *J. Atmos. Sci.* **60**(4), 667–682 (2003)
- Scott, R., Goff, J., Naveira Garabato, A., Nurser, A.: Global rate and spectral characteristics of internal gravity wave generation by geostrophic flow over topography. *J. Geophys. Res.* **116**(C9) (2011)
- Senf, F., Achatz, U.: On the impact of middle-atmosphere thermal tides on the propagation and dissipation of gravity waves. *J. Geophys. Res.* **116**(D24) (2011)
- Shaw, T.A., Shepherd, T.G.: A theoretical framework for energy and momentum consistency in subgrid-scale parameterization for climate models. *J. Atmos. Sci.* **66**(10), 3095 (2009)
- Smith, W.H.F., Sandwell, D.T.: Global seafloor topography from satellite altimetry and ship depth soundings. *Science* **277**, 1957–1962 (1997)
- Tandon, A., Garrett, C.: On a recent parameterization of mesoscale eddies. *J. Phys. Oceanogr.* **26**, 406–416 (1996)
- Thorpe, S.: The excitation, dissipation, and interaction of internal waves in the deep ocean. *J. Geophys. Res.* **80**(3), 328–338 (1975)
- von Storch, J.-S., Eden, C., Fast, I., Haak, H., Hernández-Deckers, D., Maier-Reimer, E., Marotzke, J., Stammer, D.: An estimate of the Lorenz energy cycle for the world ocean based on the STORM/NCEP simulation. *J. Phys. Oceanogr.* **42**(12), 2185–2205 (2012)
- Wang, S., Zhang, F.: Source of gravity waves within a vortex-dipole jet revealed by a linear model. *J. Atmos. Sci.* **67**(5), 1438–1455 (2010)
- Warner, C., McIntyre, M.: On the propagation and dissipation of gravity wave spectra through a realistic middle atmosphere. *J. Atmos. Sci.* **53**(22), 3213–3235 (1996)
- Warner, C., McIntyre, M.: An ultrasimple spectral parameterization for nonorographic gravity waves. *J. Atmos. Sci.* **58**(14), 1837–1857 (2001)
- Watson, K.M.: The coupling of surface and internal gravity waves: revisited. *J. Phys. Oceanogr.* **20**, 1233–1248 (1990)
- Whalen, C., Talley, L., MacKinnon, J.: Spatial and temporal variability of global ocean mixing inferred from argo profiles. *Geophys. Res. Lett.* **39**, L18612 (2012)
- Whitham, G.: Two-timing, variational principles and waves. *J. Fluid Mech.* **44**(02), 373–395 (1970)
- Williams, P.D., Haine, T.W., Read, P.L.: Inertia–gravity waves emitted from balanced flow: observations, properties, and consequences. *J. Atmos. Sci.* **65**(11) (2008)
- Wunsch, C., Ferrari, R.: Vertical mixing, energy and the general circulation of the oceans. *Annu. Rev. Fluid Mech.* **36**, 281–314 (2004)
- Yiğit, E., Aylward, A.D., Medvedev, A.S.: Parameterization of the effects of vertically propagating gravity waves for thermosphere general circulation models: Sensitivity study. *J. Geophys. Res.* **113**(D19) (2008)